GeoHealth

RESEARCH ARTICLE

10.1029/2020GH000313

Key Points:

- An optimization model coupled with dynamical downscaling is developed to improve labor productivity under intensified heat stress in China
- Civilian workers in inland regions will be more vulnerable to the intensified heat stress in a changing climate
- Compared to the regional climate model, the global climate model overestimates heat stress and thus exaggerates related system costs to recover from the working hour loss

Supporting Information:

- Supporting Information S1

Correspondence to:

S. Wang,
shuo.s.wang@polyu.edu.hk

Citation:

Zhu, J., Wang, S., Zhang, B., & Wang, D. (2021). Adapting to changing labor productivity as a result of intensified heat stress in a changing climate. *GeoHealth*, *5*, e2020GH000313. https://doi.org/10.1029/2020GH000313

Received 11 AUG 2020
Accepted 4 MAR 2021

Author Contributions:

Conceptualization: Jinxin Zhu, Shuo Wang
Data curation: Boen Zhang
Formal analysis: Jinxin Zhu, Dagang Wang
Funding acquisition: Shuo Wang
Investigation: Shuo Wang
Methodology: Jinxin Zhu
Project Administration: Shuo Wang
Resources: Shuo Wang, Boen Zhang
Supervision: Shuo Wang
Validation: Jinxin Zhu, Boen Zhang, Dagang Wang
Visualization: Jinxin Zhu
Writing – original draft: Jinxin Zhu

Adapting to Changing Labor Productivity as a Result of Intensified Heat Stress in a Changing Climate

Jinxin Zhu[1], Shuo Wang[2,3], Boen Zhang[2], and Dagang Wang[1]

[1]School of Geography and Planning, Sun Yat-Sen University, Guangzhou, China, [2]Department of Land Surveying and Geo-Informatics, The Hong Kong Polytechnic University, Hong Kong, China, [3]The Hong Kong Polytechnic University Shenzhen Research Institute, Shenzhen, China

Abstract The intensification of heat stress reduces the labor capacity and hence poses a threat to socio-economic development. The reliable projection of the changing climate and the development of sound adaptation strategies are thus desired for adapting to the decreasing labor productivity under climate change. In this study, an optimization modeling approach coupled with dynamical downscaling is proposed to design the optimal adaptation strategies for improving labor productivity under heat stress in China. The future changes in heat stress represented by the wet-bulb globe temperature (WBGT) are projected with a spatial resolution of 25 × 25 km by a regional climate model (RCM) through the dynamical downscaling of its driving global climate model (GCM). Uncertain information such as system costs, environmental costs, and subsidies are also incorporated into the optimization process to provide reliable decision alternatives for improving labor productivity. Results indicate that the intensification of WBGT is overestimated by the GCM compared to the RCM. Such an overestimation can lead to more losses in working hours derived from the GCM than those from the RCM regardless of climate scenarios. Nevertheless, the overestimated heat stress does not alter the regional measures taken to adapt to decreasing labor productivity. Compared to inland regions, the monsoon-affected regions tend to improve labor productivity by applying air conditioning rather than working overtime due to the cost differences. Consequently, decision-makers need to optimally make a balance between working overtime and air conditioning measures to meet sustainable development goals.

1. Introduction

A combination of the increasing temperature and humidity induced by climate change leads to the intensification of heat stress and thus poses a threat to human life and activities (Dunne et al., 2013; Fischer & Knutti, 2013). Exposing to the intensified heat stress directly reduces labor productivity, which has substantial impacts on economic developments and national outputs (Diffenbaugh et al., 2007; Dukesdobos, 1981; Dunne et al., 2013; Pal & Eltahir, 2015). As an important factor influencing the local development, a growing body of studies has been focusing on the assessment of climate change impacts on the labor system, and then adapting to potential impacts (Kjellstrom et al., 2009; Lee et al., 2018; Li et al., 2016; Matsumoto, 2019; Zhao et al., 2016). In previous studies, however, little effort has been devoted to designing optimal adaptation strategies to improve labor productivity. Moreover, the underlying interaction between labor productivity change and regional/local climate has not been well studied due to the most common use of the coarse-resolution global climate models (GCMs). Thus, it is much needed to integrate systems optimization and high-resolution climate projections at a regional scale for effectively improving labor productivity under climate change.

The labor system optimization generally deals with the determination of schedule patterns and workforce allocation in consideration of the availability, location, and transition. Both scheduling and planning are focused on balancing demand and availability over a short period of time. Two primary categories of planning/scheduling models for labor productivity include normative models and exploratory models (Bastian et al., 2020; Borba et al., 2019; Lavergne et al., 2019; Song & Huang, 2008). Normative models are defined as the optimization tools used to balance prescribing policies in the labor system in order to maximize labor productivity under given criteria. The ideal balance is achieved through the optimization model by exploring a certain degree of satisfaction in the objective function, such as labor size, flow, and related costs. Exploratory models are the analytical tools used to predict the change in the labor system in response to

Writing – review & editing: Shuo Wang

stationary situations. The commonly used exploratory models include renewal models (Chen et al., 2018; De Feyter et al., 2017), Markov (cross-sectional) models (Di Francesco et al., 2016; Dimitriou & Georgiou, 2019; Knorzer, 2000), and semi-Markov models (Bastian et al., 2020; Chattopadhyay & Gupta, 2007; Song & Huang, 2008). Moreover, previous studies introduced dynamic programming in a Markov model to generate optimal recruitment and transition patterns to meet various needs in labor requirements and service levels (Dimitriou & Tsantas, 2010).

Previous studies focus on the balance between the demand and availability of labor activities over a short period of time, which fails to account for the long-term climate change impacts on the labor system at national and local scales. Moreover, the related information in practical situations can be imprecise and given as intervals due to the scarcity of data, unknown technology issues, and socio-economic development. Thus, existing models with deterministic inputs and parameters are unable to address such uncertain information in the optimization process. This study aims to effectively improve the long-term labor productivity affected by climate change at a regional scale. We develop an optimization modeling approach coupled with dynamical downscaling to provide decision alternatives for improving labor productivity under uncertainty. The approach is proposed to facilitate decision-makers making informed adaptation plans for labor productivity improvement in a changing climate. Specifically, dynamical downscaling is used to develop high-resolution projections of climate variables used to assess the change of heat stress in China. Based on the projected high-resolution climate information, the interval programming model is developed to incorporate imprecise information presented as intervals into the optimization process for improving labor productivity. Interval solutions can thus be generated for decision-makers to develop informed adaptation measures with the minimum system cost in the context of climate change.

The rest of the paper is organized as follows: Section 2 presents the models and datasets used to generate high-resolution projections of heat stress and to estimate the changes in labor productivity as well as to formulate the interval programming model. Section 3 presents the high-resolution projections of heat stress, and optimal adaptation measures identified to improve labor productivity in an uncertain environment. Besides, a comparative analysis is conducted to demonstrate the added value of dynamical downscaling used to generate the high-resolution climate information at a regional scale. Section 4 concludes the novelty of the proposed approach and its practical implications for climate change mitigation and adaptation.

2. Methods and Data

2.1. Design of Experiments

The geographical complexities contribute to unique climate characteristics in different regions, which have a large impact on labor productivity. It is thus necessary to investigate the changes in labor productivity caused by regional/local climate features over different regions. The following is a Chinese case study used to demonstrate the practical significance of the proposed approach for improving labor productivity. As shown in Figure 1, China is delineated into nine climate divisions according to temperature and precipitation variabilities to better explore the regional climate impacts on labor productivity. Considering the internal regional features of precipitation in China and based on previous studies (Bucchignani et al., 2014; H. Chen et al., 2020; Guo et al., 2017; Li et al., 2015; Luo et al., 2013), we divide the contiguous China domain into nine sub-regions, namely region 1 in a cold and humid climate, region 2 in a warm and arid climate, region 3 in a cold and arid climate, region 4 in a warm and semi-arid climate, region 5 in cool and semi-humid climate, region 6 in a cool and humid climate, region 7 in a warm and humid climate, region 8 in a hot and humid climate, and region 9 in a subtropical hot and humid climate. As shown in Figure 1, these sub-regions are typically used in weather and climate-related discussions in China because of the climatic similarities within each sub-region. For each sub-region, we calculate the area-averaged temperature and relative humidity for deriving undermentioned changes in WBGT and related labor capacities.

The Providing REgional Climate Impacts for Studies (PRECIS) model version 2.0.0 developed by Met Office Hadley Center, UK was used in this study (Feng et al., 2012; Jones et al., 2004; Wang et al., 2014, 2020; Wilson et al., 2015). The PRECIS model is an atmospheric and land surface model with the dynamical flow, atmospheric sulfur cycle, clouds and precipitation, radiative processes, land surface, and deep soil described. Its ability in reproducing climatological mean and extremes over China has been widely verified

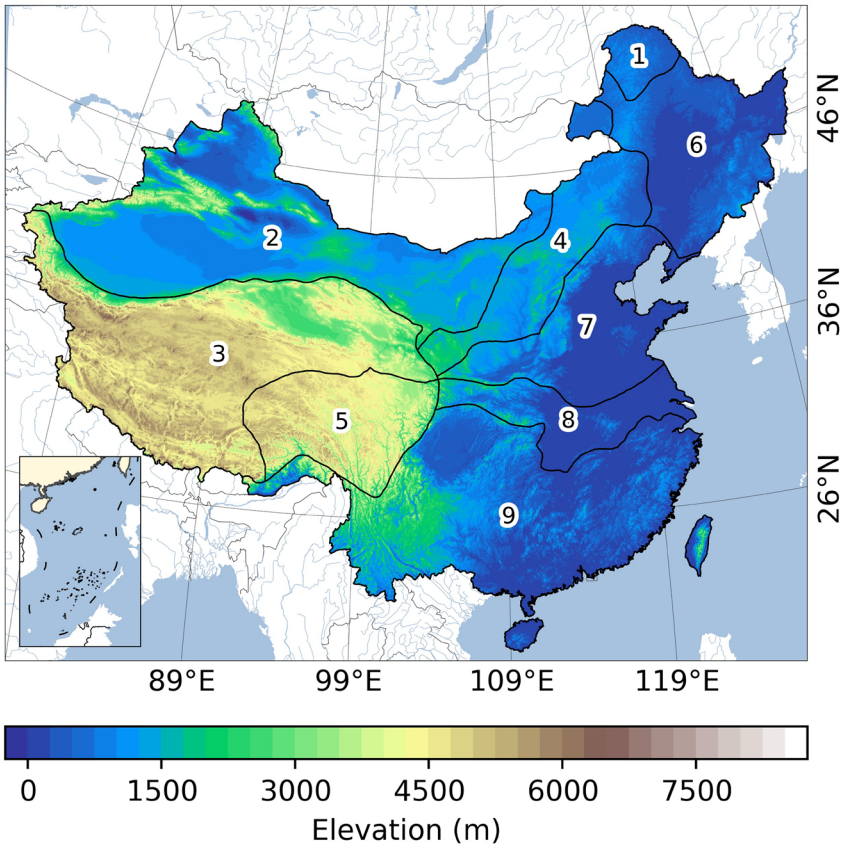

Figure 1. Nine climate divisions in China.

and tested (Wang et al., 2016; Y. Xu et al., 2009). In this study, the model simulation domain covered China and its adjacent areas with a 25 × 25 km resolution. The PRECIS runs are carried out continuously during 1969–2005 for the historical simulation and during 2006–2099 for the future projection. The computational domain of PRECIS is centered at (34°N, 105°E), and it covers China with 292 × 186 horizontal grid points and a lateral buffer zone of 20 grid points. The meteorological forcing at the limits of the PRECIS model's domain is provided by the Hadley Center Global Environment Model version 2 - Earth Systems (HadGEM2-ES) (Collins et al., 2008; C.H. Xu & Xu, 2012). The HadGEM2-ES model has a spatial resolution of 192 × 144 km (longitude by latitude) and the capability of explicitly representing biogeochemical processes that interact with the physical climate (Taylor et al., 2012). The HadGEM2-ES is a state-of-the-art earth system model which has a high climate sensitivity of ~4.6°C for a doubling of CO_2. The relatively high sensitivity to CO_2 increment makes the model at the top of the range (from 2.1°C to 4.7°C) of the CMIP5 models (Andrews et al., 2012; Caesar et al., 2013). The chance of an adaptation turning out to be inadequate can be lower when considering climate projections from models with higher sensitivity of warming to CO_2 emissions.

The WBGTs were calculated based on the HadGEM2-ES historical simulation, the PRECIS simulation, and the CRU data set over the reference period. The results, as shown in Figure 2, compare the WBGTs from two models against the WBGT from the observation over China. Compared to the WBGT derived from the CRU, we find that the area-averaged WBGT derived from the GCM simulation is higher than the value of CRU by a magnitude of 2.2°C. This is because the WBGT is the index used to reflect the combined effect of air temperature and relative humidity. As shown in Figures S1 and S2, the GCM overestimates both air temperature and relative humidity over China for the reference period compared to the observation (Zhu et al., 2017; 2019). In comparison, the RCM does better reproduce both climate variables than the GCM in terms of spatial distribution and magnitudes. But the RCM still slightly overestimates the WBGT over regions 1 and 2 and underestimates the WBGT over regions 3 and 5 (within 1°C for area averaging). As shown

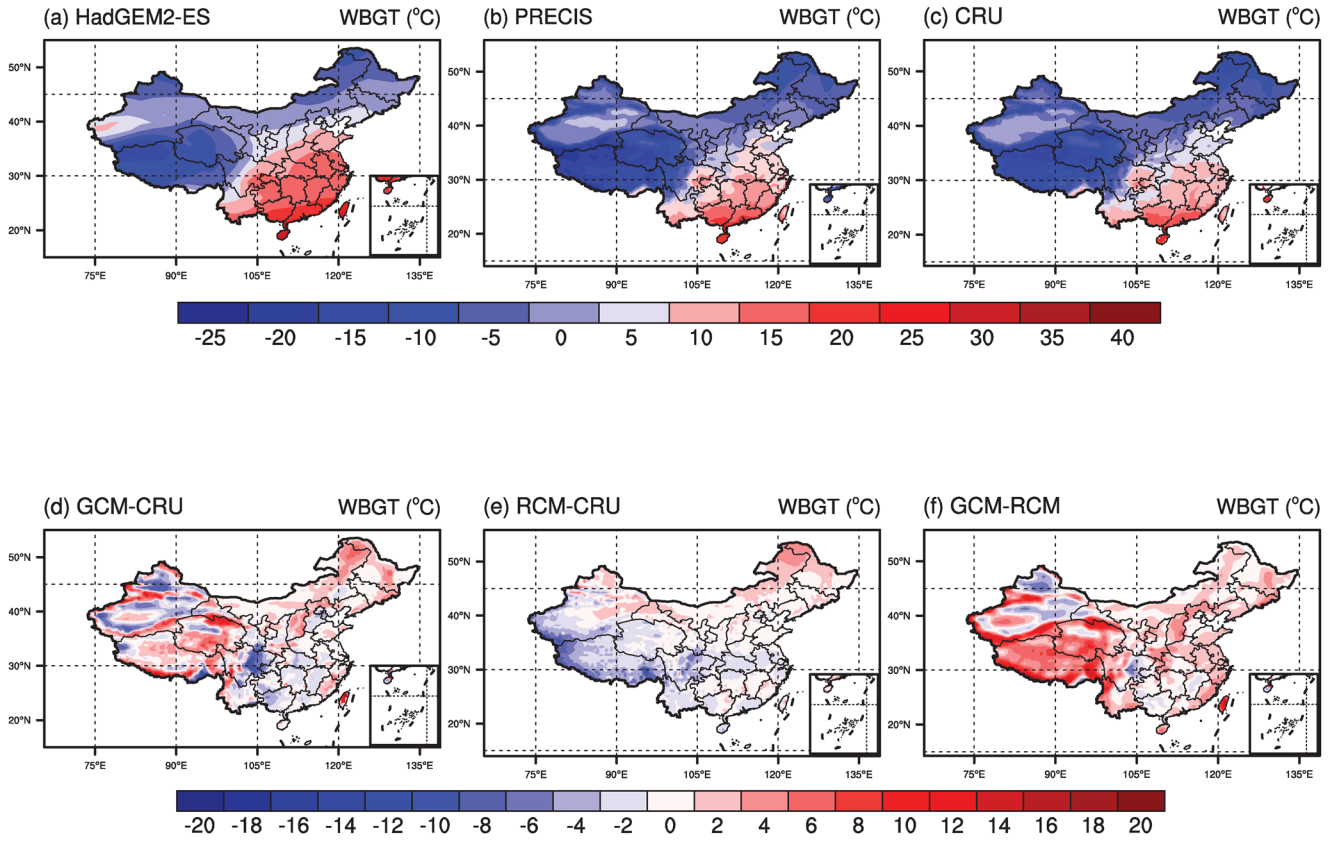

Figure 2. Spatial distributions of the annual mean WBGT (°C) from HadGEM2-ES (a), PRECIS (b), and CRU (c) and differences for GCM-CRU (d), RCM-CRU (e), and GCM-RCM (f) for the reference period (from 1981 to 2005) over China.

in the RCM-CRU differences plots of Figures S1 and S2, the PRECIS model simulates a lower temperature over regions 3 and 5 and a deficit in the moisture in region 9. To examine the skills of HadGEM2-ES and PRECIS in reproducing the WBGT, the Taylor Diagram is introduced to summarize how closely the patterns from the two models' results match the observation (Taylor, 2001). Figure 3 shows the relative merits of HadGEM2-ES and PRECIS with respect to reproducing the spatial patterns of the WBGT for nine regions. In comparison with HadGEM2-ES, results from PRECIS have CORs between 0.85 and 0.99, and SDs between 0.6 and 1.1 for all nine regions, indicating that PRECIS has reasonable performance in simulating the spatial distribution of the WBGT. One of the advantages of dynamical downscaling is reproducing and simulating the complex relationships among multiple climatic variables. The Clausius-Clapeyron relation (C-C) describes a scale of 6%–7% per K for change in water vapor with temperature by assuming constant RH near the Earth's surface. Hence, changes in variable patterns, moisture availability, and thermodynamic stability may lead to large variations in the scale. High-resolution climate models are able to simulate the scaling relationship between temperature and moisture as well as related changes under climate change (Chan et al., 2016). Relationships between hourly extreme precipitation intensities (the 90th percentile precipitation in the reference period) and daily temperatures for summer (JJA) over land points of nine regions are shown in Figure S3. For most regions, the 90th percentile precipitation increases at a rate of C-C scaling, and this scaling is captured by the PRECIS model. The GCM can capture the observed scaling but largely overestimate intensities with temperature increases. A warmer climate is more favorable to hold more moisture, but our results show that it is not always true for the warmest summer days. As seen in observational and modeling results, downturns have been found in the observed scaling at high temperatures due to the suppression of RH. The scaling declines are well captured by the RCM, while the GCM simulates the downturn point corresponding either to a higher temperature or a lower temperature. Therefore, we conclude that the RCM simulates realistic interactions between extremes by capturing the scaling of extreme precipitation with high temperatures. The PRECIS model with the ability to simulate the finer-scale

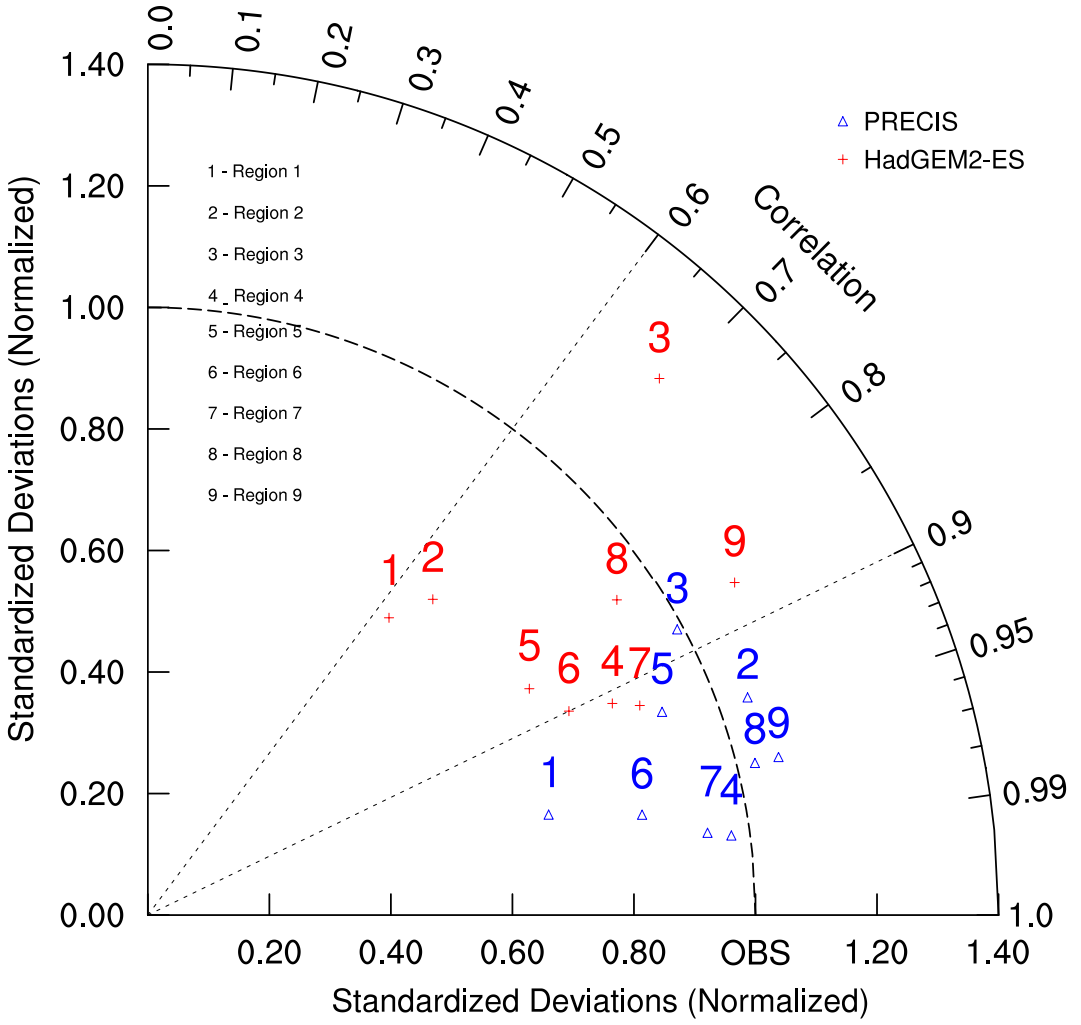

Figure 3. Comparison between model simulations and the observation of annual mean WBGTs in the Taylor Diagram.

physical processes can capture the occurrence of extreme events and better depict the interactions between extreme events over China in comparison with its driving GCM.

It is noted that the overestimation in the derived WBGT still exists in the RCM simulation without the bias correction but becomes smaller than those from the GCM. Bias-correction methods, however, could impair the advantages of climate models by altering the spatiotemporal field consistency and relations among variables as well as by largely neglecting the feedback mechanisms (Ehret et al., 2012). It could eventually lead to avoidable forejudging of decision-makers. Moreover, large model biases in simulating the present-day climate would be systematically propagated into future climate projections (Liang et al., 2008; Xue et al., 2014). To minimize the effect of model biases, future changes are assessed by subtracting the historical simulation from the future projection. In this way, the spatiotemporal field consistency and relations among climatic variables remain unchanged. In particular, the interactions between temperatures and RH are well simulated and projected by considering the feedback mechanisms. A more accurate simulation of the present-day climate provides confidence in future projections (Wang et al., 2016). Thus, meaningful information of temperatures and RH can be provided to assess the WBGT and related changes over China under different emission scenarios.

The use of daily climatic variables is essential for studying heat stress since it avoids the underestimation of extreme conditions in the monthly averaged value (Liu et al., 2018; Wang & Zhu, 2020). Daily mean surface air temperature and relative humidity were thus selected to calculate the time series of heat stress over the

reference period from 1981 to 2005 and the future period from 2076 to 2100. Various indices are also available to measure heat stress on the human body caused by the combined effect of high ambient temperature and high humidity (Fischereit & Schlünzen, 2018; Havenith & Fiala, 2016; Morabito et al., 2014). Various empirically based diagnostic metrics are developed to predict the human body's physiological responses to heat stress (Buzan et al., 2015). Limitations of diagnostic indices include lack of global-scale experiments, not well-tuned, and neglected climatic variables. Among all indices, the Wet Bulb Globe Temperature (WBGT) has the advantages of high usability and being well-validated for measuring the perceived temperature globally (Buzan & Huber, 2020; Wang & Zhu, 2020). The WBGT was adopted in this study since it was well-validated and widely used to quantify heat stress perceived by the human body. For a valid temperature range from 0°C to 100°C, the WBGT can be calculated using the Davies-Jones method (Budd, 2008; Willett & Sherwood, 2012). As we focus on investigating a low limit of heat stress in the properly sheltered/shaded daytime condition and the nighttime condition, the direct exposures to sunlight are excluded from the calculation. The equations used to estimate the WBGT are shown as follows:

$$e_{sat} = \exp(18.8764 - \frac{2991.2729}{T^2} - \frac{6017.0128}{T} - 0.0285 \times T + 1.7838 \times 10^{-5} \times T^2 - 8.4150 \times 10^{-10} \times T^3 + 4.4413 \times 10^{-13} \times T^4 + 2.8585 \times 10^{-2} \times \ln(T)) / 100. \quad (1a)$$

$$e = RH \times e_{sat}. \quad (1b)$$

$$WBGT = 0.567 \times T + 0.393 \times e + 3.94. \quad (1c)$$

where T is the daily surface air temperature (°C), RH is the relative humidity, e is the simultaneous vapor pressure (hPa), and e_{sat} is the saturation vapor pressure (hPa).

The labor capacity is the occupational capacity of safely performing continuous physical activities under environmental pressures over a certain period. The labor capacity is assumed to be 100% for a worker to safely carry out sustained labor activities without environmental pressures. The heat stress contributes to the main environmental pressure and can largely reduce the labor capacity under extreme conditions. An empirical function was formulated to estimate the relationship between WBGT and specific labor (light, moderate, and heavy labor) (Dunne et al., 2013). In the empirical function, light labor is assumed to represent roughly 50% of moderate labor, and moderate labor is assumed to represent roughly 50% of heavy labor. According to the NIOSH standard, uncertainty exists in measuring workers' tolerance for performing heavy labor under the unbearable working environment (NIOSH, 2016). In a hot environment, the threshold of labor capacity reduction for heavy labor is not deterministic, which ranges from 25°C to 26°C due to the uncertain tolerance. The threshold takes the value of 25°C when workers have a relatively low tolerance of the hot environment, and 26°C when workers have a high tolerance of the hot environment. Incorporating different tolerances of the hot environment into the modeling approach addresses the uncertainty existing in the relationship between labor capacity and heat stress. The empirical relationships between WBGT and labor capacity are demonstrated as follows:

$$LCL = \left[1 - 0.25 \times max\left(0, WBGT - 25\right)^{\frac{2}{3}}\right] \times 100\%. \quad (2a)$$

$$LCH = \left[1 - 0.25 \times max\left(0, WBGT - 26\right)^{\frac{2}{3}}\right] \times 100\%. \quad (2b)$$

where LCL is the labor capacity (%) of workers with a low tolerance of the hot environment, LCH is the labor capacity (%) of workers with a high tolerance of the hot environment, and WBGT is the wet-bulb globe temperature (°C) (WBGT).

The Bureau of Labor Statistics commonly uses four strength levels (light, moderate, heavy, and very heavy) to describe the job requirements for performing physical activities with different durations and weight

classes (*China National Bureau of Statistics*, 2020; Gong et al., 2016). For the reference period from 1981% to 2005%, 57% of Chinese civilian workers performed light level labor. 32.3% of workers were involved in moderate level activities. 9.6% and 1.1% of workers performed heavy and very heavy level activities, respectively (Liu et al., 2015; Qi et al., 2015). To be consistent with the classification of strength levels in Equation 2, the value of 10.7% (9.6% + 1.1%) was used to represent the total percentage of Chinese civilian workers involved in the heavy level activity. For each day, the labor capacity for a specified labor type can be reduced to some extent when the WBGT exceeds a threshold. The daily labor capacity reduction can be accumulated for both baseline and future periods. Thus, the accumulated labor capacity reduction for the baseline period can be subtracted from the reduction for the future period. Under normal conditions, the working hour is 8 h per day when the labor capacity is 100%. Assuming a constant heat stress effect on the hourly change in the labor capacity across all working hours, we define the annual productivity loss/working hour loss as the 25-year averaged labor capacity reduction multiplied by 8 h and the population of workers involved in a given labor type. Note that the provincial and gridded population projection for China is derived from the study by Chen et al. (2020). According to the newly published data set, the population of China is projected to decline from 1.3 billion in 2010 to 509 million by 2100. For each region, the projected population changes derived from the gridded data set are −2.4 million in region 1, −17.3 million in region 2, −3.5 million in region 3, −14.2 million in region 4, −43.8 million in region 5, −76.9 million in region 6, −165.6 million in region 7, −122.8 million in region 8, and −172.3 million in region 9. The declined population in China further aggravates the labor demands and increases the difficulty to compensate for the working hour losses caused by the intensified heat stress in the future. Considering the different heat tolerances, a working hour loss interval can be obtained with the lower bound corresponding to the threshold of 26°C and the upper bound corresponding to the threshold of 25°C.

2.2. Model Formulation

The labor productivity improvement can be considered as an interval optimization problem. The decision variables are expressed as intervals, which represent the number of working hour losses under a specific RCP scenario. The objective of the interval programing model is to recover from the lost working hours by optimally developing adaptation plans with the minimum system cost. Several adaptation measures can be implemented to restore the reduced productivity level over the planning horizon (from 2076 to 2100) to the level in the reference period. The adaptation options can be divided into two main categories, including active measures (i.e., working overtime, occupational shifts, and work practice & education programs) and passive measures (i.e., air conditioning, shades, and outdoor portable cooling devices). The model constraints are mainly derived from various restrictions on working overtime and processing capacities in the passive cooling mechanisms. It should be noted that the most passive cooling measures are carbon-emission and energy-consumption intensive solutions. Passive measures such as air conditioners consume a large amount of electricity, resulting in high CO_2 emissions in China. The use of more active measures means fewer applications of air conditioners, thereby saving energy costs. In this paper, we calculate the environmental benefits from the electricity saved by not using air conditioners. The associated environmental benefits are then included in the optimization model to achieve sustainable development goals. Active measures such as working overtime and occupational shifts often take place at nighttime. Thus, extreme events with nighttime temperatures above the threshold of labor capacity reduction could further reduce the effectiveness of these active measures to recover from the lost working hours. Such extreme conditions are also considered in the system optimization by assigning a reduction ratio to the lost working hours processed by the active measures. Labor productivity reductions induced by heat stress can decrease the value of the marginal product. The income of workers can be reduced when the value of the marginal product of labor is equal to the wage rate. When considering the wage stickiness, parts of labor can be substituted by the other agents of production (such as capital). Industries, especially the productivity in labor-intensive industries could be greatly affected by the increased heat stress, which might result in unemployment or wage reduction to workers (Jessoe et al., 2018; Mueller et al., 2014; Yu et al., 2019; Zander et al., 2016). From a long-run perspective, labors migrating to regions with low heat stress is inevitable for both preventing hazards and seeking high income. Either the short-run labor migration or the long-run migration can cause an increase in the local labor demand, which can further increase the total system cost. The detailed interval programming model is formulated as follows:

2.3. Objective Function:

$$Min\ y^{\pm} = \sum_{i=1}^{u}\sum_{j=1}^{v}\sum_{k=1}^{w} x_{ijk}^{\pm} \times \left(CI_{jk}^{\pm} + CO_{ijk}^{\pm}\right) + \sum_{i=1}^{u}\sum_{j=1}^{n}\sum_{k=1}^{w}\left[x_{ijk}^{\pm} \times \left(RT_{ik}^{\pm} \times LI_{ik}^{\pm} - EP_{ijk}^{\pm}\right)\right] + \sum_{i=1}^{u}\sum_{k=1}^{w}\left[\left(\sum_{j=1}^{n} RT_{ik}^{\pm} \times x_{ijk}^{\pm}\right) \times \left(\sum_{j=n+1}^{v} OP_{ijk}^{\pm}\right)\right] + LM_{ik}^{\pm}. \quad (3a)$$

Constraints on passive measures' capacity:

$$\sum_{i=1}^{u}\sum_{k=1}^{w}\left[\left(\sum_{j=1}^{n} RT_{ik}^{\pm} \times x_{ijk}^{\pm}\right) + \left(\sum_{j=n+1}^{v} x_{ijk}^{\pm}\right)\right] \le CP^{\pm}. \quad (3b)$$

Constraints on active measures' capacity:

$$\sum_{i=1}^{u}\sum_{j=1}^{n}\sum_{k=1}^{w} x_{ijk}^{\pm} \le CA^{\pm}. \quad (3c)$$

Constraints on the allocation of working hour losses:

$$\sum_{j=1}^{v} x_{ijk}^{\pm} = WL_{ik}^{\pm}, \forall i, k. \quad (3d)$$

$$x_{ijk}^{\pm} \ge 0, \forall i, j, k. \quad (3e)$$

where:

$y^{\pm}$ is the total system cost (unit: \$);

$x_{ijk}^{\pm}$ is the number of working hour losses in the region i allocated to the adaptation option j (Options from one to n are the active measures; Options from $n+1$ to v are the passive ones) for the labor type k (unit: hr);

$CI_{jk}^{\pm}$ is the capital investment for implementing the adaptation option j for the labor type k (unit: \$/hr);

$CO_{ijk}^{\pm}$ is the managing/operating cost for implementing the adaptation option j for the labor type k in the region i (unit: \$/hr);

$RT_{ik}^{\pm}$ is the rate of extreme events when the nighttime temperature is high enough for using passive cooling measures in the region i for the labor type k (unit: %);

$LI_{ik}^{\pm}$ is the capital investment for implementing the passive cooling measures for the labor type k in the region i during overtime/nighttime (unit: \$/hr);

$LM_{ik}^{\pm}$ is the cost for managing the labor demand change caused by the labor migration for the labor type k in the region i (unit: \$);

$OP_{ijk}^{\pm}$ is the managing/operating cost for implementing the passive cooling option j for the labor type k in the region i during overtime/nighttime (unit: \$/hr);

$EP_{ijk}^{\pm}$ is the environmental penalty saved by not using the passive cooling mechanism j for the labor type k in the region i (unit: \$/hr);

$CP^{\pm}$ is the total capacity of implementing passive measures for reversing the working hour loss (unit: hr);

$CA^{\pm}$ is the total capacity of implementing active measures for reversing the working hour loss (unit: hr);

$WL_{ik}^{\pm}$ is the accumulated working hour loss for the labor type k in the region i (unit: hr).

Solutions of the interval programming model include the objective function value $y^{\pm}$ and relevant decision variables $x_{ijk}^{\pm}, \forall i, j, k$. The objective function value can be expressed as $y^{\pm} = \left[y^{-}, y^{+}\right]$. y^{-} represents the minimum value (lower bound) of the interval system cost, and the y^{+} represents the maximum value

(upper bound). The lower and upper bounds of the objective function value correspond to decision variables $x_{ijk}^{\pm}$, $\forall i, j, k$ which can be expressed as $x_{ijk}^{\pm} = \left[x_{ijk}^{-}, x_{ijk}^{+}\right], \forall i, j, k$. The variation of decision variables within their lower and upper bounds can lead to the adjustment of the objective function value within its interval range of system cost. These solutions facilitate decision-makers in achieving cost-effective productivity improvement under different RCP scenarios. For a given RCP scenario, the interval programming model can be solved as follows:

Lower bound for the objective function:

$$\begin{aligned} Min\ y^{-} = & \sum_{i=1}^{u}\sum_{j=1}^{v}\sum_{k=1}^{w} x_{ijk}^{-} \times \left(CI_{jk}^{-} + CO_{ijk}^{-}\right) + \sum_{i=1}^{u}\sum_{j=1}^{n}\sum_{k=1}^{w}\left[x_{ijk}^{-} \times \left(RT_{ik}^{-} \times LI_{ik}^{-} - EP_{ijk}^{+}\right)\right] \\ & + \sum_{i=1}^{u}\sum_{k=1}^{w}\left[\left(\sum_{j=1}^{n} RT_{ik}^{-} \times x_{ijk}^{-}\right) \times \left(\sum_{j=n+1}^{v} OP_{ijk}^{-}\right)\right] + LM_{ik}^{-} \end{aligned} \quad (4a)$$

Constraints on passive measures' capacity:

$$\sum_{i=1}^{u}\sum_{k=1}^{w}\left[\left(\sum_{j=1}^{n} RT_{ik}^{-} \times x_{ijk}^{-}\right) + \left(\sum_{j=n+1}^{v} x_{ijk}^{-}\right)\right] \le CP^{+}. \quad (4b)$$

Constraints on active measures' capacity:

$$\sum_{i=1}^{u}\sum_{j=1}^{n}\sum_{k=1}^{w} x_{ijk}^{-} \le CA^{+}. \quad (4c)$$

Constraints on the allocation of working hour losses:

$$\sum_{j=1}^{v} x_{ijk}^{-} = WL_{ik}^{-}, \forall i, k. \quad (4d)$$

$$x_{ijk}^{-} \ge 0, \forall i, j, k. \quad (4e)$$

Let $x_{ijk_{opt}}^{-}$ be the solution of the model given in function (4a)-(4e).

Upper bound for the objective function:

$$\begin{aligned} Min\ y^{+} = & \sum_{i=1}^{u}\sum_{j=1}^{v}\sum_{k=1}^{w} x_{ijk}^{+} \times \left(CI_{jk}^{+} + CO_{ijk}^{+}\right) + \sum_{i=1}^{u}\sum_{j=1}^{n}\sum_{k=1}^{w}\left[x_{ijk}^{+} \times \left(RT_{ik}^{+} \times LI_{ik}^{+} - EP_{ijk}^{-}\right)\right] \\ & + \sum_{i=1}^{u}\sum_{k=1}^{w}\left[\left(\sum_{j=1}^{n} RT_{ik}^{+} \times x_{ijk}^{+}\right) \times \left(\sum_{j=n+1}^{v} OP_{ijk}^{+}\right)\right] + LM_{ik}^{+} \end{aligned} \quad (5a)$$

Constraints on passive measures' capacity:

$$\sum_{i=1}^{u}\sum_{k=1}^{w}\left[\left(\sum_{j=1}^{n} RT_{ik}^{+} \times x_{ijk}^{+}\right) + \left(\sum_{j=n+1}^{v} x_{ijk}^{+}\right)\right] \le CP^{-}. \quad (5b)$$

Constraints on active measures' capacity:

$$\sum_{i=1}^{u}\sum_{j=1}^{n}\sum_{k=1}^{w} x_{ijk}^{+} \le CA^{-}. \quad (5c)$$

Constraints on the allocation of working hour loss:

$$\sum_{j=1}^{v} x_{ijk}^{+} = WL_{ik}^{+}, \forall i, k. \quad (5d)$$

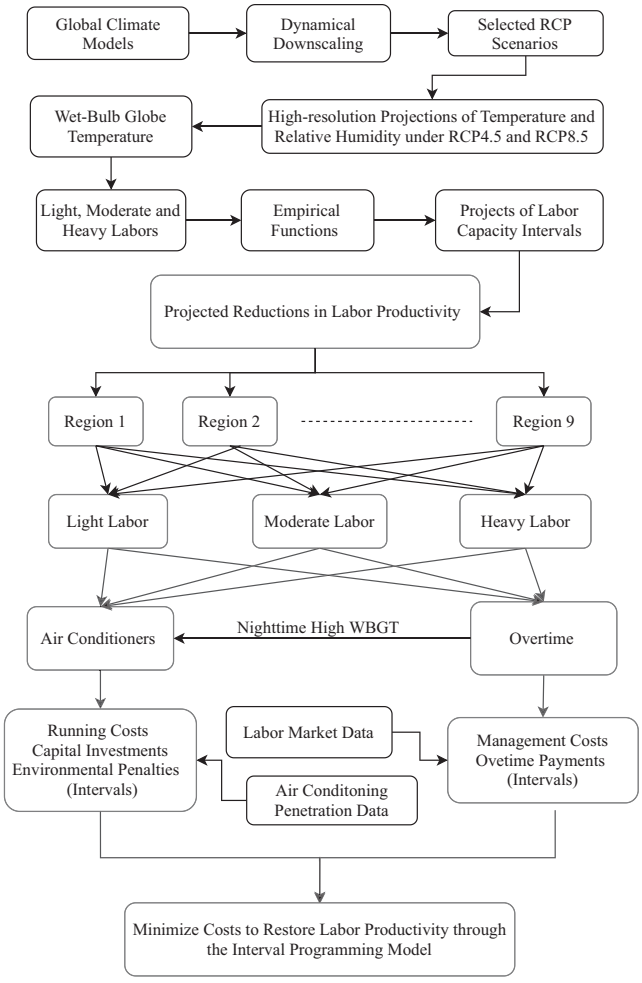

Figure 4. Flow chart for the proposed systems optimization modeling approach coupled with dynamical downscaling.

$$x_{ijk}^{+} \geq 0, \forall i, j, k. \tag{5e}$$

$$x_{ijk}^{+} \geq x_{ijkopt}^{-}, \forall i, j, k. \tag{5f}$$

Figure 4 shows the framework of the proposed optimization modeling approach for improving labor productivity under climate change. First, the coarse-resolution GCM is dynamically downscaled to obtain the high-resolution climate information over China under two RCP scenarios. Second, the high-resolution climate projections are used to generate the daily time series of WBGT. Third, the empirical function considering different tolerances of the hot environment is applied to reveal the changes in the labor capacity and to address related uncertainties (presented as intervals). Fourth, a combination of labor capacity changes and socio-economic drivers is taken into account to predict future working hour losses under two RCPs. Fifth, the uncertain information related to climate change and the costs in labor systems are incorporated into an interval programming model to provide optimal solutions for achieving productivity improvement with the minimum system cost.

3. Results and Discussion

3.1. Projection of Heat Stress Changes

Figure 5 shows the projected changes in heat stress represented by the WBGT above 25°C (which is the threshold of labor capacity reduction for workers with a low heat tolerance), derived from the GCM and RCM for the end of the 21st century relative to the reference period under RCP4.5 and RCP8.5 (for the changes in the WBGT above 26°C, please refer to the Figure S4). For both models, the WBGT is projected to increase across China with different spatial patterns and magnitudes under RCP4.5 and RCP8.5. Both models simulate a 2.26°C increase in the WBGT under RCP4.5 and a 4.12°C increase under RCP8.5 over all the land areas except the Tibetan Plateau in China. The Tibetan Plateau has a low temperature in the past and a slight increase in the future WBGT due to its high altitude. Plus, the RCM simulates a relatively low WBGT over regions 3 and 5 compared to the observation. Based on the comparison between the RCM and its driving GCM, as shown in Figures 5c and 5f, the increase in the WBGT derived from the GCM is larger than those from the RCM despite a large variation in the spatial distribution of the WBGT change. Specifically, the increase in the WBGT is 1.30°C for regions 1, 4, and 6, and 0.02°C for regions 7, 8, and 9 under RCP4.5. Under RCP8.5, the increase in the WBGT is 1.26°C for most regions in China. Overall, the WBGT increase derived from the GCM is 1.19°C higher than the increment from the RCM. Our previous studies show that regional climate downscaling improves the simulation of relative humidity as well as minimum and maximum temperatures over China. The driving GCM does capture the spatial patterns but holistically overestimates air temperature and relative humidity. Large model biases in simulating the present-day climate would be systematically propagated into future climate projections at regional scales (Liang et al., 2008; Xue et al., 2014; Zhang et al., 2021). The RCM simulates the WBGT relatively low over the Tibetan Plateau which could result in potential underestimations in labor capacity reduction. While the GCM projection can result in an overestimation of the WBGT above the threshold of labor capacity reduction and hence exaggerate the labor capacity reduction compared to the RCM projection.

As shown in Figure S4, the projected positive changes in the WBGT above 26°C (which is the threshold of labor capacity reduction for workers with a high heat tolerance) have higher values derived from the GCM than those from the RCM. The slight cold bias of the RCM could lead to an underestimation

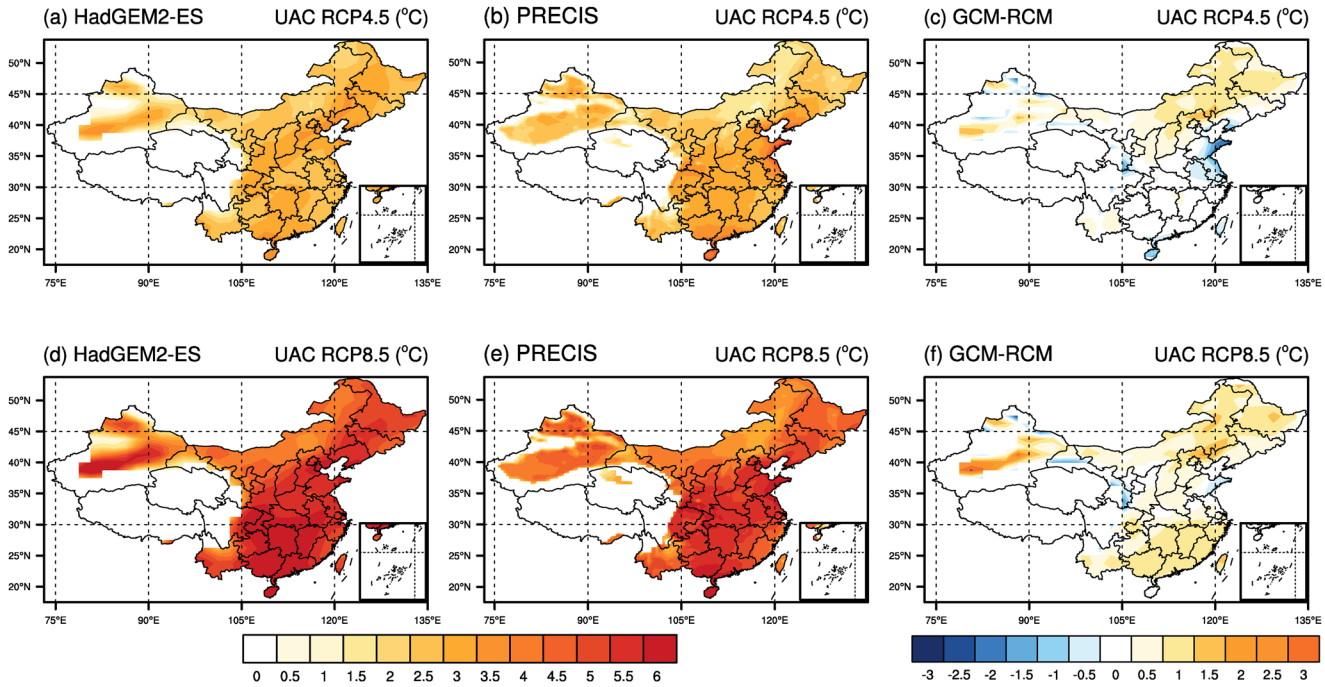

Figure 5. Projected changes in the daily WBGT (°C) above 25°C (which is the threshold of labor capacity reduction for workers with a low heat tolerance) derived from the driving GCM and the RCM, and the differences between two models under RCP4.5 and RCP8.5 for the end of the 21st century relative to the baseline period (white areas represent no value).

in the WBGT projection. Since the Tibetan Plateau has a low temperature due to its high latitude, the overestimated WBGT is still projected to be below the threshold of labor productivity reduction. The potential risk of underestimated labor productivity reduction over the Tibetan Plateau is small and can be neglected. The larger warm bias of the GCM can be further propagated into the projections and thus cause an overestimation in the WBGT calculation. In addition, the GCM fails to capture some variations in the spatial distribution of the WBGT changes due to its coarse resolution, whereas the RCM depicts detailed geographical features in the WBGT change. For instance, the WGBT is relatively high over the Tarim Basin and the Qaidam Basin because of high air temperature and relative humidity in the low altitude and not well-ventilated areas. With the high-resolution simulation and better representation of the topography, the RCM is able to capture all these fine-scale changes in the WBGT over both basins, while some parts of Tarim Basin and the whole Qaidam Basin are simulated with no changes by the GCM. Despite these differences detected in the spatial patterns of the WBGT increases between the two models, we find a consistent intensification of heat stress across the whole country under two RCPs except the Tibetan Plateau.

3.2. Projected Changes in Labor Capacities and Working Hour Losses under Heat Stress

Figures 6 and 7 show the projected changes in labor capacities for workers with low and high heat tolerances for the 2076–2100 period relative to the baseline period under RCP8.5 (for the results under RCP4.5, please refer to the Figures S5 and S6). Both the GCM and RCM simulate a large reduction in the accumulated labor capacity for light, moderate, and heavy labor types all over China except for the Tibetan Plateau (regions 3 and 5) under two RCPs. The largest labor capacities can be over 600 h per year for all three labor types under both RCPs. But the spatial distribution of the largest reduction in labor capacities varies with the labor types and shows a different pattern for a selected model. For a specific labor type, the GCM projects a larger reduction in labor capacities than the RCM due to the overestimation of future WBGT changes (i.e., labor capacity reductions over the entire region 4, the Tarim Basin in region 2, as well as the Zhejiang Province and the Fujian Province in region 9 for the light and moderate labor types). This is because the model bias of the GCM is larger than the RCM, which is propagated into future climate projections. The warm biases of

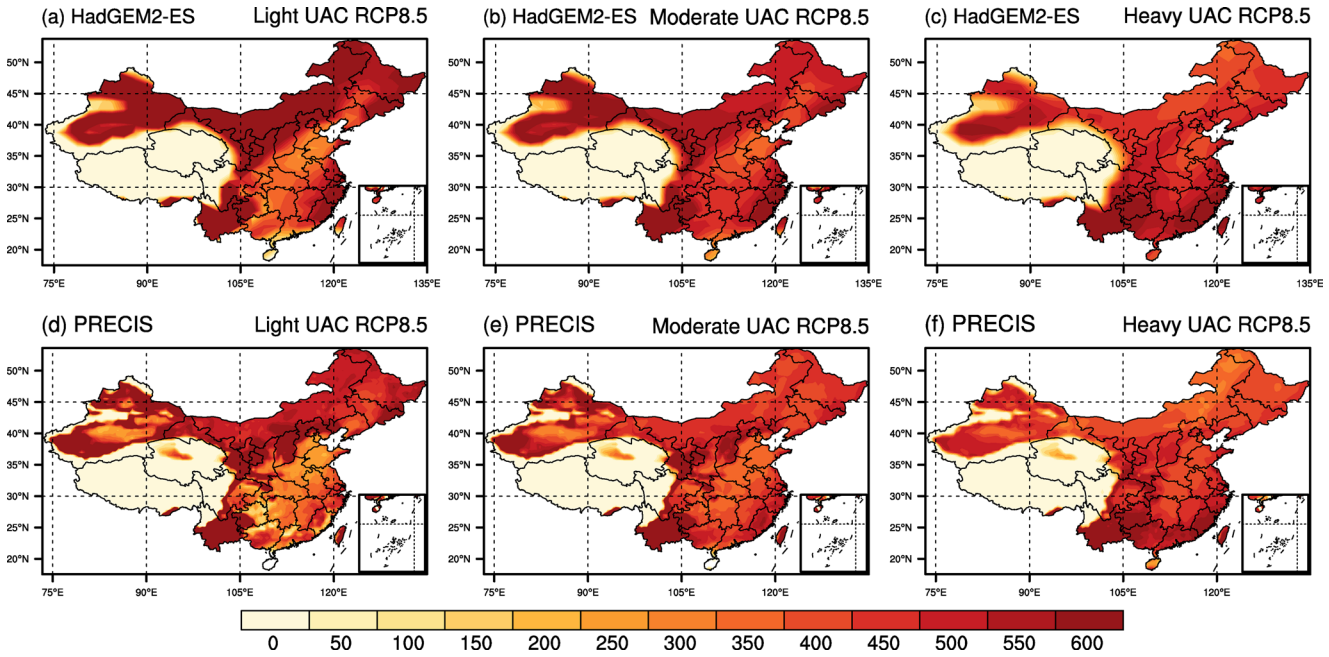

Figure 6. Projected labor capacity reductions (hr) for workers with a low heat tolerance (25°C) in terms of three different labor types, derived from the GCM (a–c) and the RCM (d–f) under RCP8.5.

the GCM can be largely reduced in the RCM through better representation of geographical complexity and finer-scale physical processes (J. X. Zhu et al., 2018; Zhu et al., 2019). Therefore, the reliability of assessing labor capacity reductions can be improved with the high-resolution projection.

It should be noted that there is a distinct difference between labor capacity reductions in inland areas (regions 1, 2, and 4) and monsoon-affected areas (regions 6, 7, 8, and 9) for both RCM and its driving GCM. For all three labor activity types, it is notable that large working hour losses are taking place in the southern and

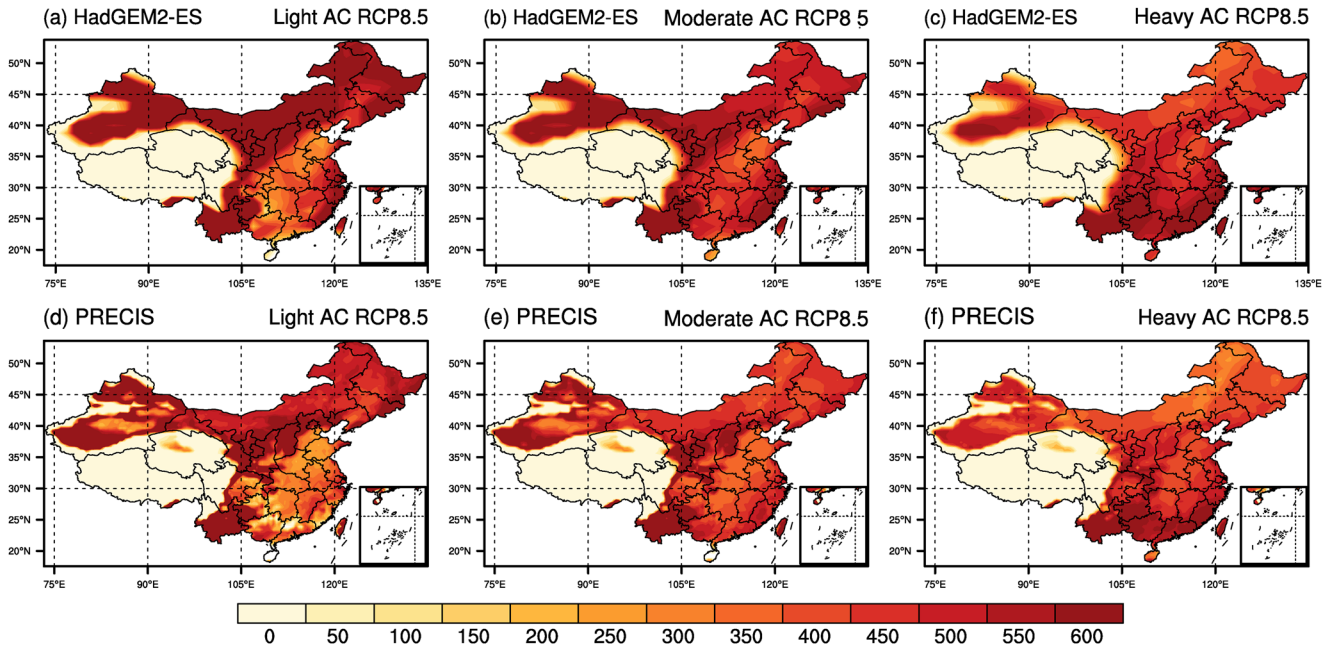

Figure 7. Projected labor capacity reductions (hr) for workers with a high heat tolerance (26°C) in terms of three different labor types, derived from the GCM (a–c) and the RCM (d–f) under RCP8.5.

eastern parts of region 9. It is because that the relatively small warming can easily make temperature above the threshold of productivity reduction for year-round high temperatures. For light and moderate types, results indicate that large working hour losses happen in arid and semi-arid areas such as regions 2, 4, and 7. The reason behind this phenomenon is the combined effect of a high proportion of the working population and a large increase in accumulated working hour losses. Climate warming further aggravates the drying situation in these arid and semi-arid areas in China. With reduced precipitation and increased temperature, it is more likely to develop prolonged heatwaves and cause surges in the accumulated working hour losses at the end of the 21st century. With the air temperature rising rapidly, the dry areas tend to become drier, and the wet areas become wetter. The air temperature is about 0.7°C higher under RCP4.5 and 1°C higher under RCP8.5 for the inland areas compared to monsoon-affected areas. As for the relative humidity, there are about a 7% difference under RCP 4.5 and 15% difference under RCP8.5 for the inland areas compared to monsoon-affected areas. This results in more prolonged heatwaves (13% increase in frequency under RCP4.5 and 16% increase in frequency under RCP8.5) with temperatures exceeding the thresholds of labor capacity reduction in these regions. Considering the disproportionate population of workers involved in three labor types, the light labor activities have the largest labor capacity reduction, and the heavy labor activities have the least reduction. As shown in Figure S7, light labor has the highest threshold (30°C) of labor capacity reduction, moderate labor has the second-largest threshold (28°C), and heavy labor has the lowest threshold (25°C). Therefore, the largest labor capacity reduction for the light labor activities results from the largest population of civilian workers involved.

Table 1 shows the intervals of total working hour losses estimated for three labor types in nine regions under two RCP scenarios. There is a distinct difference between inland areas and monsoon-affected areas in terms of working hour losses. The monsoon-affected areas have greater working hour losses than the inland areas for all three labor types. The relatively large working hour losses in monsoon-affected areas result from the combination of the dense population and the large labor capacity reduction. Figure 8 shows the ranges between the lower and upper bounds of future working hour losses caused by workers' different heat tolerances under RCP8.5 (for the results under RCP4.5, please refer to Figure S8). Through the comparison between the two models, we find that the spatial pattern of the interval ranges of future working hour losses is difficult to interpret due to a mixture of uncertainties in model projections and the complex relationship between heat stress and labor capacity as well as the difference in the population of workers involved in various labor types. Despite different types of labor activities, we find that the ranges derived from the GCM projection vary largely from those estimated by the RCM over nine regions of China. For the cold and humid region 1, the RCM enlarges the range of working hour losses in comparison to the GCM for all three labor types. For the arid regions (regions 2 and 4), the RCM ranges are narrower than the GCM ranges for the moderate and heavy labor types. For the warm and humid regions (regions 6 and 7), ranges from the RCM become smaller than the ranges from the GCM for three labor types. For the hot and humid regions (regions 8 and 9), the RCM ranges are larger than the GCM ranges, especially for region 8.

3.3. Optimal Schemes for Improving Labor Productivity under Uncertainty

In China, the increased working hour losses caused by intensified heat stress already have a significant impact on social and economic development (Zhao et al., 2016). Various adaptation options (include but not limited to air conditioning, outdoor shades, green roofs, working overtime, early heat warning systems, and education/awareness campaigns) are available to mitigate or even reverse the negative impacts of climate change on labor productivity. As mentioned in Section 2, systematic planning of adaptation strategies for improving labor productivity is complicated and can be affected by various uncertainties from climate change projection and socio-economic development. For instance, considerable uncertainty existing in the implementation of adaptation measures results from direct and indirect costs including investment, operation, maintenance, and management costs. It is thus necessary to incorporate various uncertain information into systematic planning to effectively design the optimal adaptation strategies. Based on the rules of thumb, the two most cost-effective adaptation measures can be taken to recover from working hour losses, namely air conditioning and working overtime (Day et al., 2019). Therefore, systems optimization of air conditioning and working overtime measures for improving labor productivity has the most significant implication for adaptation to climate change in China. Table 2 shows the economic costs presented as intervals

Table 1
Intervals of Working Hour Losses for Three Labor Types, Derived From the GCM and the RCM Under RCP4.5 and RCP8.5

		RCP4.5 (million hours)		RCP8.5 (million hours)	
Regions	Labor types	GCM	RCM	GCM	RCM
Region 1	Light	[1,241, 1,337]	[981, 1,043]	[2,070, 2,108]	[1,812, 1,851]
	Moderate	[995, 1,057]	[789, 854]	[1,711, 1,754]	[1,478, 1,536]
	Heavy	[705, 769]	[578, 634]	[1,340, 1,408]	[1,162, 1,231]
Region 2	Light	[28,363, 30,263]	[27,100, 27,738]	[50,498, 51,600]	[41,902, 43,536]
	Moderate	[23,019, 24,451]	[22,089, 22,380]	[41,378, 42,749]	[36,105, 36,686]
	Heavy	[17,074, 18,447]	[17,903, 18,366]	[32,586, 34,401]	[31,404, 31,953]
Region 3	Light	[0, 1]	[9, 22]	[8, 19]	[122, 179]
	Moderate	[1, 3]	[18, 35]	[16, 30]	[126, 175]
	Heavy	[3, 5]	[24, 38]	[22, 38]	[104, 139]
Region 4	Light	[33,791, 34,026]	[27,454, 27,996]	[51,552, 52,672]	[45,801, 46,079]
	Moderate	[26,309, 26,847]	[21,972, 22,588]	[41,809, 42,054]	[38,389, 38,744]
	Heavy	[19,119, 20,187]	[16,611, 17,568]	[33,116, 34,254]	[31,421, 32,510]
Region 5	Light	[4, 9]	[24, 55]	[352, 768]	[397, 595]
	Moderate	[15, 31]	[49, 98]	[573, 974]	[429, 625]
	Heavy	[45, 108]	[70, 115]	[627, 945]	[401, 584]
Region 6	Light	[39,313, 41,391]	[34,632, 36,062]	[60,935, 64,203]	[55,643, 56,914]
	Moderate	[33,225, 34,272]	[29,779, 30,366]	[54,066, 55,866]	[50,280, 50,777]
	Heavy	[29,188, 29,283]	[25,901, 26,284]	[49,977, 50,044]	[45,679, 46,032]
Region 7	Light	[105,898, 112,464]	[92,255, 102,918]	[159,577, 171,108]	[151,960, 160,199]
	Moderate	[106,646, 109,306]	[97,033, 101,909]	[167,056, 173,008]	[161,230, 165,767]
	Heavy	[108,129, 109,537]	[104,036, 105,861]	[176,449, 180,129]	[171,205, 173,835]
Region 8	Light	[43,440, 43,756]	[47,661, 53,204]	[71,793, 71,962]	[71,501, 77,307]
	Moderate	[46,806, 47,168]	[48,692, 51,529]	[79,167, 79,500]	[76,552, 79,251]
	Heavy	[49,273, 49,786]	[52,275, 53,473]	[83,761, 84,312]	[82,306, 84,114]
Region 9	Light	[196,001, 220,664]	[159,234, 183,822]	[330,206, 335,961]	[304,189, 314,498]
	Moderate	[190,181, 197,585]	[176,928, 187,739]	[310,093, 314,217]	[302,380, 305,192]
	Heavy	[173,990, 176,305]	[177,228, 178,545]	[298,083, 300,079]	[293,069, 293,833]

Abbreviations: GCM, global climate model; RCM, regional climate model.

for implementing air conditioning and working overtime measures over the planning horizon (25 years). These intervals reflect the uncertainty in the implementation of adaptation measures and vary with primary drivers including population projection, economic development, and technology development. We use the provincial-level air conditioning penetration rate, the market value of the air conditioner and the averaged energy consumption reported in the China Statistics Yearbook for the baseline period (China National Bureau of Statistics, 2020). The running costs and capital investments for the future application of air conditioning are estimated based on historical statistics and projected changes in the primary drivers. Based on the national regulations, population projections, and GDP (Gross National Product) predictions, the managing costs and the payments for working overtime are also estimated accordingly (please refer to the supplementary information for more details).

All the intervals can be incorporated into the interval programming model formulated in Section 2. We find that the regions with dense populations and developed economies (i.e., monsoon-affected regions 7, 8, and

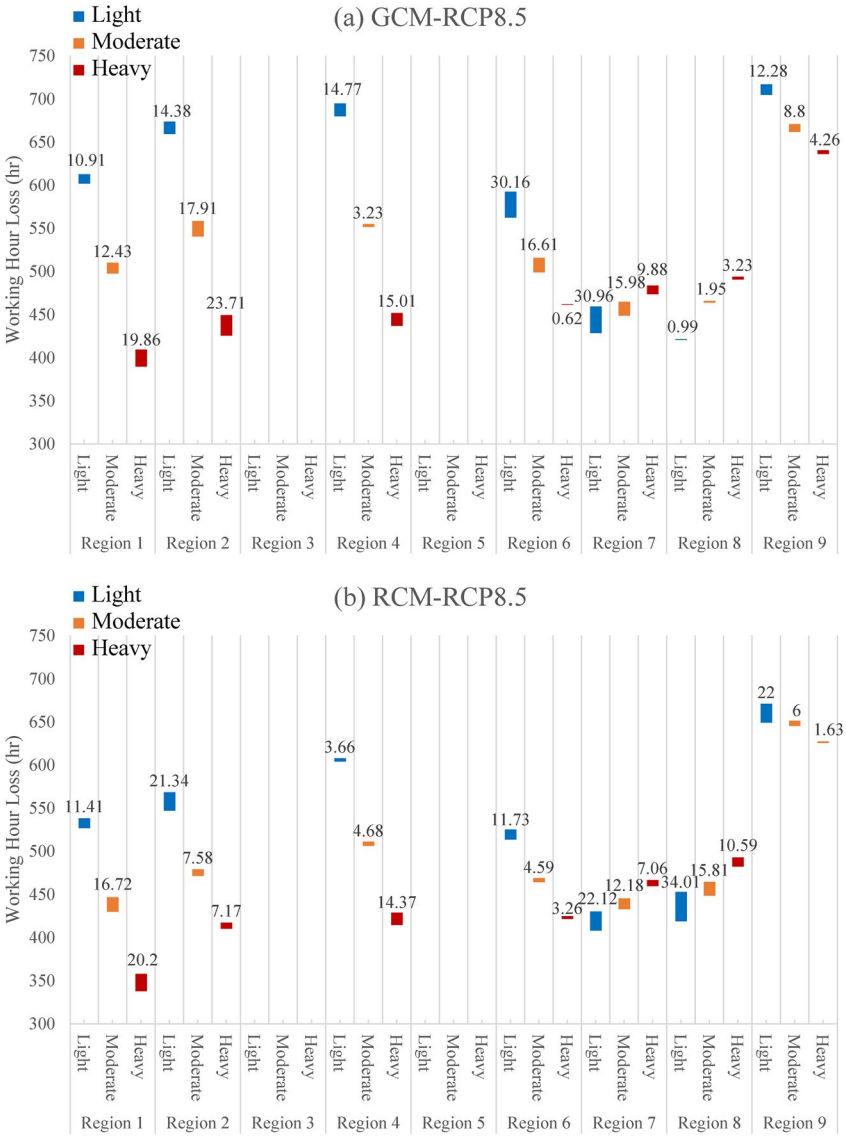

Figure 8. Ranges between the lower and upper bounds of future working hour losses for three labor types, derived from the GCM (a) and the RCM (b) under RCP8.5.

9) have higher overtime costs than the other regions. Since there is no big difference among all regions in terms of the market value and the electricity consumption of air conditioning, the capital investment for the passive cooling measure is directly linked to the local air conditioning penetration rate. A high penetration rate indicates a relatively low cost for increasing the application of air conditioners in the future. Regions with a hot and humid climate in China already have relatively high air conditioning penetration rates in the baseline period. Therefore, these regions will have relatively low capital investments for adaptation to the amplified heat stress than the other regions in a changing climate. It should be noted that a high penetration rate also represents a large energy consumption, and hence a high running cost. By considering various constraints of processing capacities in adaptation options and by choosing different combinations of working hour allocations within their interval ranges, a set of decision alternatives can be generated to improve labor productivity with the minimum system cost as well as to address the underlying uncertainties in both climate and labor systems. The following is the interval programming model applied to China for demonstrating the feasibility of the proposed modeling approach:

Table 2
Costs of Implementing Air Conditioning and Working Overtime Over the Planning Period

		Air conditioning ($/hr)		Overtime ($/hr)	
Regions	Labor types	Running costs	Costs	Managing costs	Payments
1	Light	[1.555, 3.373]	[33.768, 37.798]	[4.742, 6.063]	[30.099, 34.370]
	Moderate	[2.212, 4.699]	[34.368, 39.293]	[5.321, 6.987]	[34.222, 37.150]
	Heavy	[0.253, 1.757]	[30.125, 34.082]	[2.650, 5.504]	[28.678, 32.055]
2	Light	[4.843, 6.749]	[41.250, 45.697]	[9.822, 12.333]	[39.324, 42.671]
	Moderate	[4.442, 7.525]	[50.359, 55.330]	[10.636, 12.391]	[43.173, 46.082]
	Heavy	[2.793, 4.864]	[41.248, 45.857]	[7.695, 9.996]	[37.022, 40.647]
4	Light	[4.753, 6.687]	[44.254, 49.009]	[10.301, 12.738]	[43.984, 47.712]
	Moderate	[7.648, 9.678]	[46.197, 50.890]	[11.904, 13.140]	[47.936, 53.448]
	Heavy	[2.782, 3.741]	[38.328, 42.799]	[9.170, 11.873]	[40.791, 45.045]
6	Light	[5.176, 7.393]	[40.534, 45.798]	[11.455, 13.140]	[55.055, 60.035]
	Moderate	[8.366, 10.256]	[42.154, 46.782]	[11.747, 13.801]	[60.035, 62.890]
	Heavy	[5.788, 6.765]	[40.273, 44.147]	[10.307, 11.518]	[53.433, 56.522]
7	Light	[7.508, 9.236]	[43.607, 48.469]	[14.685, 18.169]	[71.796, 75.127]
	Moderate	[10.268, 12.336]	[54.211, 58.881]	[14.524, 18.398]	[71.858, 76.969]
	Heavy	[6.286, 7.861]	[39.896, 44.783]	[11.845, 14.163]	[67.985, 73.384]
8	Light	[6.467, 9.986]	[52.105, 56.502]	[15.306, 19.123]	[71.811, 75.638]
	Moderate	[9.491, 11.795]	[55.002, 60.140]	[14.144, 17.495]	[73.208, 76.980]
	Heavy	[5.867, 7.622]	[43.593, 47.252]	[11.881, 15.949]	[71.099, 76.367]
9	Light	[8.800, 10.641]	[53.264, 58.395]	[17.208, 21.014]	[82.160, 85.972]
	Moderate	[11.819, 14.726]	[59.386, 63.834]	[15.229, 19.236]	[87.022, 90.044]
	Heavy	[7.792, 9.048]	[45.839, 49.708]	[12.426, 15.044]	[77.167, 81.507]

Objective function:

$$Min\ y^{\pm} = \sum_{i=1}^{7}\sum_{j=1}^{2}\sum_{k=1}^{3} x_{ijk}^{\pm} \times \left(CI_{jk}^{\pm} + CO_{ijk}^{\pm}\right) + \sum_{i=1}^{7}\sum_{k=1}^{3}(RT_{ik}^{\pm} \times x_{i1k}^{\pm} \times LI_{ik}^{\pm} + RT_{ik}^{\pm} \times x_{i1k}^{\pm} \times OP_{i2k}^{\pm} - x_{i1k}^{\pm} \times EP_{i1k}^{\pm}). \tag{6a}$$

Constraints on air conditioning's capacity:

$$\sum_{i=1}^{7}\sum_{k=1}^{3}\left(RT_{ik}^{\pm} \times x_{i1k}^{\pm} + x_{i2k}^{\pm}\right) \le CP^{\pm}. \tag{6b}$$

Constraints on overtime's capacity:

$$\sum_{i=1}^{7}\sum_{k=1}^{3} x_{i1k}^{\pm} \le CA^{\pm}. \tag{6c}$$

Constraints on the allocation of working hour losses:

$$\sum_{j=1}^{2} x_{ijk}^{\pm} = WL_{ik}^{\pm}, \forall i, k. \tag{6d}$$

$$x_{ijk}^{\pm} \ge 0, \forall i, j, k. \tag{6e}$$

According to the solving procedure introduced in Section 2.2, the interval programming model can be solved in the following steps. First, the interval programming model can be converted into two deterministic sub-models that correspond to the upper and lower bounds of the system cost. Second, the sub-model representing the lower-bound system cost is solved first because the objective function is to find the minimum value of system costs. The optimal solutions $x_{ijk}^{-}{}_{opt}$ derived from the first sub-model will serve as constraints for the second sub-model representing the upper-bound system cost. Third, the second sub-model is solved to obtain the optimal solutions $x_{ijk\ opt}^{+}$ for the objective function. Last, steps 1–3 are repeated to generate optimal solutions for developing cost-effective adaptation plans under a different RCP scenario. For a specific RCP scenario, the computational processes are shown as follows:

Lower bound for the objective function:

$$\begin{aligned} Min\ y^{-} \quad = \quad & \sum_{i=1}^{7}\sum_{j=1}^{2}\sum_{k=1}^{3} x_{ijk}^{-} \times \left(CI_{jk}^{-} + CO_{ijk}^{-}\right) + \sum_{i=1}^{7}\sum_{k=1}^{3}(RT_{ik}^{-} \times x_{i1k}^{-} \times LI_{ik}^{-} + RT_{ik}^{-} \times x_{i1k}^{-} \times OP_{i2k}^{-} \\ & - x_{i1k}^{-} \times EP_{i1k}^{+}) \end{aligned} \tag{7a}$$

Constraints on air conditioning's capacity:

$$\sum_{i=1}^{7}\sum_{k=1}^{3}\left(x_{i2k}^{-} + RT_{ik}^{-} \times x_{i1k}^{-}\right) \le CP^{+}. \tag{7b}$$

Constraints on overtime's capacity:

$$\sum_{i=1}^{7}\sum_{k=1}^{3} x_{i1k}^{-} \le CA^{+}. \tag{7c}$$

Constraints on the allocation of working hour losses:

$$\sum_{j=1}^{2} x_{ijk}^{-} = WL_{ik}^{-}, \forall i, k. \tag{7d}$$

$$x_{ijk}^{-} \ge 0, \forall i, j, k. \tag{7e}$$

Let $x_{ijk_{opt}}^{-}$ be the solution of the model given in function (7a)-(7e).

Upper bound for the objective function:

$$Min\ y^{+} = \sum_{i=1}^{7}\sum_{j=1}^{2}\sum_{k=1}^{3} x_{ijk}^{+} \times \left(CI_{jk}^{+} + CO_{ijk}^{+}\right) + \sum_{i=1}^{7}\sum_{k=1}^{3}\left(RT_{ik}^{+} \times x_{i1k}^{+} \times LI_{ik}^{+} + RT_{ik}^{+} \times x_{i1k}^{+} \times OP_{i2k}^{+} - x_{i1k}^{+} \times EP_{i1k}^{-}\right). \tag{8a}$$

Constraints on air conditioning's capacity:

$$\sum_{i=1}^{7}\sum_{k=1}^{3}\left(x_{i2k}^{+} + RT_{ik}^{+} \times x_{i1k}^{+}\right) \le CP^{-}. \tag{8b}$$

Constraints on overtime's capacity:

$$\sum_{i=1}^{7}\sum_{k=1}^{3} x_{i1k}^{+} \le CA^{-}. \tag{8c}$$

Constraints on the allocation of working hour losses:

$$\sum_{j=1}^{2} x_{ijk}^{+} = WL_{ik}^{+}, \forall i, k. \tag{8d}$$

Table 3
Solutions for Improving Labor Productivity With the Minimum Cost Derived From the GCM and the RCM Under RCP4.5

		GCM (million hours)		RCM (million hours)	
Regions	Labor types	Overtime	Air conditioning	Overtime	Air conditioning
Region 1	Light	[0, 0]	[1,241, 1,337]	[0, 0]	[981, 1,043]
	Moderate	[995, 1,057]	[0, 0]	[789, 854]	[0, 0]
	Heavy	[705, 769]	[0, 0]	[578, 634]	[0, 0]
Region 2	Light	[0, 0]	[28,363, 30,263]	[0, 0]	[27,100, 27,738]
	Moderate	[23,019, 23,019]	[0, 1432]	[22,089, 22,089]	[0, 291]
	Heavy	[17,074, 18,447]	[0, 0]	[17,903, 18,366]	[0, 0]
Region 4	Light	[0, 0]	[33,791, 34,026]	[0, 0]	[27,454, 27,996]
	Moderate	[0, 0]	[26,309, 26,847]	[0, 0]	[21,972, 22,588]
	Heavy	[0, 0]	[19,119, 20,187]	[0, 0]	[16,611, 17,568]
Region 6	Light	[0, 0]	[39,313, 41,391]	[0, 0]	[34,632, 36,062]
	Moderate	[0, 0]	[33,225, 34,272]	[0, 0]	[29,779, 30,366]
	Heavy	[0, 0]	[29,188, 29,283]	[0, 0]	[25,901, 26,284]
Region 7	Light	[33,124, 33,124]	[72,774, 79,340]	[19,481, 19,481]	[72,774, 83,437]
	Moderate	[33,872, 33,872]	[72,774, 75,434]	[24,259, 24,259]	[72,774, 77,650]
	Heavy	[44,193, 44,194]	[63,935, 65,343]	[39,077, 39,078]	[64,958, 66,783]
Region 8	Light	[0, 0]	[43,440, 43,756]	[0, 0]	[47,661, 53,204]
	Moderate	[0, 0]	[46,806, 47,168]	[0, 0]	[48,692, 51,529]
	Heavy	[0, 0]	[49,273, 49,786]	[0, 0]	[52,275, 53,473]
Region 9	Light	[154,033, 168,414]	[41,967, 52,249]	[108,075, 115,782]	[51,159, 68,039]
	Moderate	[117,407, 118,513]	[72,774, 79,071]	[104,154, 106,206]	[72,774, 81,532]
	Heavy	[126,520, 126,521]	[47,470, 49,785]	[130,567, 130,568]	[46,660, 47,977]

Abbreviations: GCM, global climate model; RCM, regional climate model.

$$x_{ijk}^{+} \geq 0, \forall i, j, k. \tag{8e}$$

$$x_{ijk}^{+} \geq x_{ijkopt}^{-}, \forall i, j, k. \tag{8f}$$

Tables 3 and 4 show the solutions (i.e., values for decision variables) obtained from both GCM and RCM for improving labor productivity with the minimum cost under RCP4.5 and RCP8.5. Several solutions are deterministic numbers with equivalent lower- and upper-bound values. This implies that these decision variables are insensitive to the uncertainties in model parameters and constraints. In general, the deterministic solutions include $x_{111}^{\pm}$, $x_{122}^{\pm}$, $x_{123}^{\pm}$, $x_{211}^{\pm}$, $x_{223}^{\pm}$, $x_{411}^{\pm}$, $x_{412}^{\pm}$, $x_{413}^{\pm}$, $x_{611}^{\pm}$, $x_{612}^{\pm}$, $x_{613}^{\pm}$, $x_{811}^{\pm}$, $x_{812}^{\pm}$, $x_{813}^{\pm}$ with values of 0, and $x_{212}^{\pm}$, $x_{711}^{\pm}$, $x_{712}^{\pm}$ with values larger than 0 for both models under RCP4.5 and RCP8.5. The distribution of deterministic solutions for the decision variables from the GCM is identical to the distribution generated from the RCM under both RCPs. Since both models under two RCPs utilize the same economic data of adaptation implementation costs, the pattern of allocating working hours to adaptation options is determined by the costs of implementing the adaptation measures rather than the difference in the accumulated working hour losses. For a selected decision variable, its solution has a larger value (for either lower or upper bound) based on the GCM results than the RCM results, and under RCP8.5 than under RCP4.5. It indicates that there are less working hour losses projected by the RCM under the medium-emission scenario (RCP4.5). Regardless of the climate scenario uncertainty, solutions derived from the RCM are less likely exaggerated than those from the GCM. This is because the dynamical downscaling approach improves the reliability of future projections by incorporating the fine-scale physical processes into the model simulation.

Table 4
Solutions for Improving Labor Productivity With the Minimum Cost Derived From the GCM and the RCM Under RCP8.5

		GCM (million hours)		RCM (million hours)	
Regions	Labor types	Overtime	Air conditioning	Overtime	Air conditioning
Region 1	Light	[0, 0]	[2,070, 2,108]	[0, 0]	[1,812, 1,851]
	Moderate	[1,711, 1,754]	[0, 0]	[1,478, 1,536]	[0, 0]
	Heavy	[1,340, 1,408]	[0, 0]	[1,162, 1,231]	[0, 0]
Region 2	Light	[0, 0]	[50,498, 51,600]	[0, 0]	[41,902, 43,536]
	Moderate	[41,378, 41,378]	[0, 1,371]	[36,105, 36,105]	[0, 581]
	Heavy	[32,586, 34,401]	[0, 0]	[31,404, 31,953]	[0, 0]
Region 4	Light	[0, 0]	[51,552, 52,672]	[0, 0]	[45,801, 46,079]
	Moderate	[0, 0]	[41,809, 42,054]	[0, 0]	[38,389, 38,744]
	Heavy	[0, 0]	[33,116, 34,254]	[0, 0]	[31,421, 32,510]
Region 6	Light	[0, 0]	[60,935, 64,203]	[0, 0]	[55,643, 56,914]
	Moderate	[0, 0]	[54,066, 55,866]	[0, 0]	[50,280, 50,777]
	Heavy	[0, 0]	[49,977, 50,044]	[0, 0]	[45,679, 46,032]
Region 7	Light	[19,577, 19,577]	[140,000, 151,531]	[11,960, 11,960]	[140,000, 148,239]
	Moderate	[27,056, 27,056]	[140,000, 145,952]	[21,230, 21,230]	[140,000, 144,537]
	Heavy	[45,561, 45,562]	[130,888, 134,567]	[39,006, 39,007]	[132,199, 134,828]
Region 8	Light	[0, 0]	[71,793, 71,962]	[0, 0]	[71,501, 77,307]
	Moderate	[0, 0]	[79,167, 79,500]	[0, 0]	[76,552, 79,251]
	Heavy	[0, 0]	[83,761, 84,312]	[0, 0]	[82,306, 84,114]
Region 9	Light	[237,758, 237,758]	[92,449, 98,203]	[205,236, 205,237]	[98,953, 109,261]
	Moderate	[170,093, 170,093]	[140,000, 144,124]	[162,380, 162,380]	[140,000, 142,812]
	Heavy	[197,604, 197,604]	[100,479, 102,475]	[191,336, 191,337]	[101,733, 102,496]

Abbreviations: GCM, global climate model; RCM, regional climate model.

In China, most regions use the air conditioning measure up to its limits for all labor types due to the relatively low operating costs. When the limitations of the processing capacity of air conditioning are exceeded, overtime measures are then applied to compensate for the working hour losses. Under RCP4.5, the air conditioning option will process [721,763, 760,971] hours based on the GCM projection and [714,158, 773,561] hours based on the RCM projection. The overtime measure will process [550,944, 567,930] hours based on the GCM and [466,973, 477,318] hours based on the RCM. Under RCP8.5, the air conditioning measure will process [1,339,869, 1,366,798] hours based on the GCM and [1,294,170, 1,322,560] hours based on the RCM. As for the overtime measure, it will process [701,976, 776,591] hours based on the GCM and [701,298, 774,664] hours based on the RCM. Overall, we find that the air conditioning processes more working hour losses than the overtime measure for both models under two RCPs. It should be noted that the carbon footprint and energy consumption will be increased by largely applying air conditioning to improve labor productivity. However, heat-related work injuries can be reduced because of peaks of heat stress smoothed by the air conditioning measure. In this study, the related costs for work injuries and fatalities with the increased exposure to heat stress were not considered due to insufficient health data in China. Finally, we obtain the optimal minimum system cost $y^{\pm}$ through the interval programming model to improve the productivity levels of light, moderate, and heavy labor. Total system costs are [26,969, 38,344] billion dollars derived from the GCM model under RCP4.5, [23,005, 32,603] billion dollars from the RCM under RCP 4.5, [38,855, 53,172] billion dollars from the GCM under RCP8.5, and [35,655, 48,675] billion dollars from the RCM under RCP8.5. We can further notice that the interval value of the system cost derived from the GCM is consistently larger than the value derived from the RCM under both RCPs. For a regional study, it could lead to an exaggerated labor productivity reduction and the related budget waste for recovering from losses without a reliable projection of heat stress.

Figure 9. Decision alternatives for achieving labor productivity recovery with the minimum cost, obtained from the GCM and the RCM under RCP4.5.

To further examine the local impacts on implementing adaptation measures, the regional preferences to process working hour losses are plotted in Figures 9 and 10. On one hand, the inland regions with low air conditioning penetration rates and less developed economies (such as regions 1, 2, and 4) tend to improve the productivity level by applying overtime rather than the air conditioning under two RCP scenarios. This is because these regions have relatively low temperatures in the past, high costs for air conditioning, and low overtime costs for all types of labor activities. On the other hand, the monsoon-affected regions 7, 8, and 9 tend to improve labor productivity by air conditioning rather than by working overtime. These warm and hot regions have more needs of using air conditioning due to the relatively high temperature, the high overtime cost due to the well-developed economies, and the low cost to use air conditioning due to the high penetration rates of air conditioning. Moreover, civilian workers in these regions are more likely to have experienced extreme heat days in the baseline period and hence are more adaptive to the intensified heat stress than the workers in inland areas in the future. Therefore, actions are more urgently needed for inland areas to improve the workplace environment by increasing air conditioning applications and to reduce the workers' exposure to the intensified heat stress. Effective air conditioning adoption policies should be developed within safe emissions budgets.

4. Conclusions

In this study, an optimization modeling approach coupled with dynamical downscaling is developed for the first time to improve labor productivity for adaptation to the intensified heat stress in a changing climate. The approach merges the strengths of the high-resolution projection of climate variables through dynamical downscaling and an interval programming model designed to systematically perform productivity recovery under uncertainty. The daily time series of air temperature and relative humidity are extracted from climate simulations to estimate heat stress represented by the WBGT. The projected daily WBGT is used to calculate the labor capacity change through the empirical relationship between heat stress and labor capacity. Different heat tolerances are considered by the modeling approach to reflect the uncertainty in

Figure 10. Decision alternatives for achieving labor productivity recovery with the minimum cost, obtained from the GCM and the RCM under RCP8.5.

the empirical relationship and to generate a plausible range of labor capacity reduction. The labor capacity range combined with socio-economic projections is then employed to calculate working hour loss intervals which serve as decision variables in the established interval programming model. Decision alternatives to optimally improve labor productivity are obtained by solving the interval programming model under uncertainty. In addition, a comparison between the GCM and the RCM is conducted to investigate the difference in the projected heat stress and the related change in labor productivity. Our study has the following implications for improving labor productivity in a changing climate: (i) understanding various uncertainties in climate and labor systems; (ii) quantifying the impact of climate change on labor productivity at a regional/local scale; (iii) developing robust tools to incorporate uncertainties into the decision-making process; (iv) developing a systematical framework for improving labor productivity with a potential to extend to other countries.

A Chinese case study is introduced in this paper to demonstrate the practical significance of the novel approach for improving labor productivity under climate change and estimating the related economic consequences. Results indicate that both GCM and RCM simulate an increase in heat stress, which leads to a large decrease in the labor capacity over China except for the Tibetan Plateau. Although biases still exist in both models, we highlight that the overestimation in the heat stress increase and the labor productivity reduction, which are caused by model biases, can be reduced by increasing the model resolution through dynamically downscaling. Compared to the RCM, the large bias of the GCM can result in the exaggeration in labor productivity reduction. Such an exaggerated reduction could cause a budget waste for planning productivity recovery, thereby largely increasing the overall system cost. The minimum system costs are [26,969, 38,344] billion dollars based on the GCM projection under RCP4.5, [23,005, 32,603] billion dollars based on the RCM under RCP4.5, [38,855, 53,172] billion dollars based on the GCM under RCP8.5, and [35,655, 48,675] billion dollars based on the RCM under RCP8.5. The system costs based on the GCM projection are consistently larger than those based on the RCM under both RCPs. We highlight the necessity of using the dynamical downscaling approach to achieve a reliable projection of heat stress for a regional study of the labor productivity restoration. Regardless of the difference caused by the

dynamical downscaling approach, monsoon-affected regions should have more productivity recovered by the air conditioning than the working overtime option to minimize the system cost. On the contrary, the inland regions tend to have their lost working hours recovered by working overtime instead of expanding the air conditioning scale to save their budgets. This is because the pattern of allocating working hours to adaptation options is determined by the costs of implementing the adaptation measures through the interval programming model. The well-developed economy and the high air conditioning penetration rate can lead to high overtime costs and low costs of air conditioning. Moreover, since inland regions in China are not heat-prone areas, civilian workers in these regions experience less extreme heat days in the baseline period and hence are more vulnerable to the intensified heat stress than the workers in monsoon-affected regions in the future period. Therefore, actions are urgently needed for the inland regions to improve the workplace environment by increasing air conditioning applications and reducing the workers' exposure to the intensified heat stress. Decision-makers also need to design effective adaptation policies to optimally make a balance between air conditioning and working overtime measures to achieve sustainable development goals.

Conflict of Interest

The authors declare no conflicts of interest relevant to this study.

Data Availability Statement

Readers can find the data that support or underlie the conclusions presented in the Mendeley Data (http://dx.doi.org/10.17632/fwygmxxpjh.1).

Acknowledgments
This research was supported by the National Natural Science Foundation of China (Grant No. 51809223) and the Hong Kong Research Grants Council Early Career Scheme (Grant No. PP5Z). The authors would like to express their sincere gratitude to the editor and anonymous reviewers for their constructive comments and suggestions.

References

Andrews, T., Gregory, J. M., Webb, M. J., & Taylor, K. E. (2012). Forcing, feedbacks and climate sensitivity in CMIP5 coupled atmosphere-ocean climate models. *Geophysical Research Letters*, *39*. https://doi.org/10.1029/2012GL051607

Bastian, N. D., Lunday, B. J., Fisher, C. B., & Hall, A. O. (2020). Models and methods for workforce planning under uncertainty: Optimizing US Army cyber branch readiness and manning. *OMEGA - The International Journal of Management Science*, *92*. https://doi.org/10.1016/j.omega.2019.102171

Borba, B. S. M. C., Fortes, M. Z., Bitencourt, L. A., Ferreira, V. H., Maciel, R. S., Guimaraens, M. A. R., et al. (2019). A review on optimization methods for workforce planning in electrical distribution utilities. *Computers & Industrial Engineering*, *135*, 286–298. https://doi.org/10.1016/j.cie.2019.06.002

Bucchignani, E., Montesarchio, M., Cattaneo, L., Manzi, M. P., & Mercogliano, P. (2014). Regional climate modeling over China with COSMO-CLM: Performance assessment and climate projections. *Journal of Geophysical Research - D: Atmospheres*, *119*, 151–212. https://doi.org/10.1002/2014JD022219

Budd, G. M. (2008). Wet-bulb globe temperature (WBGT)-its history and its limitations. *Journal of Science and Medicine in Sport*, *11*(1), 20–32. https://doi.org/10.1016/j.jsams.2007.07.003

Buzan, J. R., & Huber, M. (2020). Moist heat stress on a hotter earth. *Annual Review of Earth and Planetary Sciences*, *48*(1), 623–655. https://doi.org/10.1146/annurev-earth-053018-060100

Buzan, J. R., Oleson, K., & Huber, M. (2015). Implementation and comparison of a suite of heat stress metrics within the Community Land Model version 4.5. *Geoscientific Model Development*, 8, 151–170. https://doi.org/10.5194/gmd-8-151-2015

Caesar, J., Palin, E., Liddicoat, S., Lowe, J., Burke, E., Pardaens, A., et al. (2013). Response of the HadGEM2 earth system model to future greenhouse gas emissions pathways to the year 2300*. *Journal of Climate*, *26*, 3275–3284. https://doi.org/10.1175/jcli-d-12-00577.1

Chan, S. C., Kendon, E. J., Roberts, N. M., Fowler, H. J., & Blenkinsop, S. (2016). Downturn in scaling of UK extreme rainfall with temperature for future hottest days. *Nature Geosciences*, *9*, 24. https://doi.org/10.1038/ngeo2596

Chattopadhyay, A. K., & Gupta, A. (2007). A stochastic manpower planning model under varying class sizes. *Annals of Operations Research*, *155*(1), 41–49. https://doi.org/10.1007/s10479-007-0208-y

Chen, C. H., Yan, S. Y., & Chen, M. (2018). Short-term manpower planning for MRT carriage maintenance under mixed deterministic and stochastic demands (vol 181, pg 67, 2010). *Annals of Operations Research*, *264*(1–2), 543. https://doi.org/10.1007/s10479-017-2703-0

Chen, H., Wang, S., Zhu, J., & Zhang, B. (2020). Projected changes in abrupt shifts between dry and wet extremes over China through an ensemble of regional climate model simulations. *Journal of Geophysical Research: Atmospheres*, *125*(23), e2020JD033894. https://doi.org/10.1029/2020jd033894

China National Bureau of Statistics, (2020). *China statistics Yearbook*. China Statistics Press.

Collins, W. J., Bellouin, N., Doutriaux-Boucher, M., Gedney, N., Hinton, T., Jones, C. D., et al. (2008). *Evaluation of the HadGEM2 model. Met Office Hadley Center Technical Note no. HCTN 74, available from Met Office, FitzRoy Road, Exeter EX1 3PB*. Retrieved from http://www.metoffice.gov.uk/publications/HCTN/index.html

Day, E., Fankhauser, S., Kingsmill, N., Costa, H., & Mavrogianni, A. (2019). Upholding labor productivity under climate change: An assessment of adaptation options. *Climate Policy*, *19*(3), 367–385. https://doi.org/10.1080/14693062.2018.1517640

De Feyter, T., Guerry, M.-A., & Komarudin, (2017). Optimizing cost-effectiveness in a stochastic Markov manpower planning system under control by recruitment. *Annals of Operations Research*, *253*(1), 117–131. https://doi.org/10.1007/s10479-016-2311-4

Di Francesco, M., Díaz-Maroto Llorente, N., Zanda, S., & Zuddas, P. (2016). An optimization model for the short-term manpower planning problem in transhipment container terminals. *Computers & Industrial Engineering*, *97*, 183–190. https://doi.org/10.1016/j.cie.2016.04.012

Diffenbaugh, N. S., Pal, J. S., Giorgi, F., & Gao, X. (2007). Heat stress intensification in the Mediterranean climate change hotspot. *Geophysical Research Letters*, *34*(11). https://doi.org/10.1029/2007gl030000

Dimitriou, V. A., & Georgiou, A. C. (2019). *Introduction, analysis and asymptotic behavior of a multi-level manpower planning model in a continuous time setting under potential department contraction, Communications*. Statistics-Theory M.

Dimitriou, V. A., & Tsantas, N. (2010). Evolution of a time dependent Markov model for training and recruitment decisions in manpower planning. *Linear Algebra Application*, *433*(11–12), 1950–1972. https://doi.org/10.1016/j.laa.2010.07.001

Dukes-Dobos, F. N. (1981), Hazards of heat exposure. A review, *Scandinavian Journal of Work, Environment & Health*, *7*(2), 73–83. https://doi.org/10.5271/sjweh.2560

Dunne, J. P., Stouffer, R. J., & John, J. G. (2013). Reductions in labor capacity from heat stress under climate warming. *Nature Climate Change*, *3*(6), 563–566. https://doi.org/10.1038/Nclimate1827

Ehret, U., Zehe, E., Wulfmeyer, V., Warrach-Sagi, K., & Liebert, J. (2012). HESS Opinions "Should we apply bias correction to global and regional climate model data?". *Hydrology and Earth System Sciences*, *16*, 3391–3404. https://doi.org/10.5194/hess-16-3391-2012

Feng, J.-M., Wang, Y.-L., Ma, Z.-G., & Liu, Y.-H. (2012). Simulating the regional impacts of urbanization and anthropogenic heat release on climate across China. *Journal of Climate*, *25*(20), 7187–7203. https://doi.org/10.1175/JCLI-D-11-00333.1

Fischer, E. M., & Knutti, R. (2013). Robust projections of combined humidity and temperature extremes. *Nature Climate Change*, *3*(2), 126–130. https://doi.org/10.1038/Nclimate1682

Fischereit, J., & Schlünzen, K. H. (2018). Evaluation of thermal indices for their applicability in obstacle-resolving meteorology models. *International Journal of Biometeorology*, *62*(10), 1887–1900. https://doi.org/10.1007/s00484-018-1591-6

Gong, Y., Huo, Y., & Cccp (2016). A survey of national cardiology workforce in China. *European Heart Journal - Supplements*, *18*(A), A1–A5. https://doi.org/10.1093/eurheartj/suw002

Guo, J., Huang, G., Wang, X., Li, Y., & Lin, Q. (2017). Investigating future precipitation changes over China through a high-resolution regional climate model ensemble. *Earth's Future*, *5*, 285–303. https://doi.org/10.1002/2016EF000433

Havenith, G., & Fiala, D. (2016). Thermal indices and thermophysiological modeling for heat stress. *Comprehensive Physiology*, *6*(1), 255–302. https://doi.org/10.1002/cphy.c140051

Jessoe, K., Manning, D. T., & Taylor, J. E. (2018). Climate change and labor allocation in rural Mexico: Evidence from annual fluctuations in weather. *The Economic Journal*, *128*(608), 230–261. https://doi.org/10.1111/ecoj.12448

Jones, R. G., Noguer, M., Hassell, D. C., Hudson, D., Wilson, S. S., Jenkins, G. J., & Mitchell, J. F. (2004). *Generating high resolution climate change scenarios using PRECIS*. Met Office Hadley Centre.

Kjellstrom, T., Kovats, R. S., Lloyd, S. J., Holt, T., & Tol, R. S. J. (2009). The direct impact of climate change on regional labor productivity. *Archives of Environmental & Occupational Health*, *64*(4), 217–227. https://doi.org/10.1080/19338240903352776

Knorzer, M. (2000). *Models for manpower planning including temporary labor contracts to overcome shortages of personal in the IT industry*. Wirtschaftsinf. S36-+.

Lavergne, M. R., Goldsmith, L. J., Grudniewicz, A., Rudoler, D., Marshall, E. G., Ahuja, M., et al. (2019). Practice patterns among early-career primary care (ECPC) physicians and workforce planning implications: Protocol for a mixed methods study. *Bmj Open*, *9*(9). https://doi.org/10.1136/bmjopen-2019-030477

Lee, S.-W., Lee, K., & Lim, B. (2018). Effects of climate change-related heat stress on labor productivity in South Korea. *International Journal of Biometeorology*, *62*(12), 2119–2129. https://doi.org/10.1007/s00484-018-1611-6

Li, X., Chow, K. H., Zhu, Y., & Lin, Y. (2016). Evaluating the impacts of high-temperature outdoor working environments on construction labor productivity in China: A case study of rebar workers. *Building and Environment*, *95*, 42–52. https://doi.org/10.1016/j.buildenv.2015.09.005

Li, X., Zhou, W., & Chen, Y. D. (2015). Assessment of regional drought trend and risk over China: A drought climate division perspective. *Journal of Climate*, *28*, 7025–7037. https://doi.org/10.1175/jcli-d-14-00403.1

Liang, X.-Z., Kunkel, K. E., Meehl, G. A., Jones, R. G., & Wang, J. X. L. (2008). Regional climate models downscaling analysis of general circulation models present climate biases propagation into future change projections. *Geophysical Research Letters*, *35*, L08709. https://doi.org/10.1029/2007GL032849

Liu, X., Tang, Q., Zhang, X., & Sun, S. (2018). Projected changes in extreme high temperature and heat stress in China. *Journal of Meteorological Research*, *32*(3), 351–366. https://doi.org/10.1007/s13351-018-7120-z

Liu, X. L., Liu, S. S., & Wang, H. L. (2015). Workforce differentiation and human resource management practices: An exploratory research in China. The *Anthropologist*, *21*(3), 450–460.

Luo, L., Tang, W., Lin, Z., & Wood, E. F. (2013). Evaluation of summer temperature and precipitation predictions from NCEP CFSv2 retrospective forecast over China. *Clim Dynamics*, *41*, 2213–2230. https://doi.org/10.1007/s00382-013-1927-1

Matsumoto, K. I. (2019). Climate change impacts on socioeconomic activities through labor productivity changes considering interactions between socioeconomic and climate systems. *Journal of Cleaner Production*, *216*, 528–541. https://doi.org/10.1016/j.jclepro.2018.12.127

Morabito, M., Crisci, A., Messeri, A., Capecchi, V., Modesti, P. A., Gensini, G. F., & Orlandini, S. (2014). Environmental temperature and thermal indices: What is the most effective predictor of heat-related mortality in different geographical contexts? *Scientific World Journal*. https://doi.org/10.1016/96175010.1155/2014/961750

Mueller, V., Gray, C., & Kosec, K. (2014). Heat stress increases long-term human migration in rural Pakistan. *Nature Climate Change*, *4*(3), 182–185. https://doi.org/10.1038/nclimate2103

NIOSH. (2016). *NIOSH criteria for a recommended standard: Occupational exposure to heat and hot environments*. U.S. Department of Health and Human Services, Centers for Disease Control and Prevention, National Institute for Occupational Safety and Health, DHHS (NIOSH) Publication.

Pal, J. S., & Eltahir, E. A. B. (2015). Future temperature in southwest Asia projected to exceed a threshold for human adaptability. *Nature Climate Change*, *6*(2). https://doi.org/10.1038/nclimate2833

Qi, X., Wang, Y., Xia, L., Meng, Y., Li, Y., Yu, S., et al. (2015). Cross-sectional survey on public health informatics workforce in China: Issues, developments and the future. *Public Health*, *129*(11), 1459–1464. https://doi.org/10.1016/j.puhe.2015.03.002

Song, H., & Huang, H.-C. (2008). A successive convex approximation method for multistage workforce capacity planning problem with turnover. *European Journal of Operational Research*, *188*(1), 29–48. https://doi.org/10.1016/j.ejor.2007.04.018

Taylor, K. E. (2001). Summarizing multiple aspects of model performance in a single diagram. *Journal of Geophysical Research*, *106*, 7183–7192. https://doi.org/10.1029/2000JD900719

Taylor, K. E., Stouffer, R. J., & Meehl, G. A. (2012). An overview of CMIP5 and the experiment design. *Bulletin of the American Meteorological Society*, *93*(4), 485–498. https://doi.org/10.1175/Bams-D-11-00094.1

Wang, S., & Zhu, J. X. (2020). Amplified or exaggerated changes in perceived temperature extremes under global warming. *Climate Dynamics*, *54*(1–2), 117–127. https://doi.org/10.1007/s00382-019-04994-9

Wang, S., Zhu, J. X., Huang, G., Baetz, B., Cheng, G., Zeng, X., & Wang, X. (2020). Assessment of climate change impacts on energy capacity planning in Ontario, Canada using high-resolution regional climate model. *Journal of Cleaner Production*, *274*, 123026. https://doi.org/10.1016/j.jclepro.2020.123026

Wang, X., Huang, G., & Liu, J. (2014). Projected increases in near-surface air temperature over Ontario, Canada: A regional climate modeling approach. *Climate Dynamics*, *45*, 1381. https://doi.org/10.1007/s00382-014-2387-y

Wang, X., Huang, G., & Liu, J. (2016). Twenty-first century probabilistic projections of precipitation over Ontario, Canada through a regional climate model ensemble. *Climate Dynamics*, *46*, 3979. https://doi.org/10.1007/s00382-015-2816-6

Willett, K. M., & Sherwood, S. (2012). Exceedance of heat index thresholds for 15 regions under a warming climate using the wet-bulb globe temperature. *International Journal of Climatology*, *32*(2), 161–177. https://doi.org/10.1002/joc.2257

Wilson, W., Hassell, D., Hein, D., Wang, C., Tucker, S., Jones, R., & Taylor, R. (2015). *Technical manual for PRECIS: The Met Office Hadley Center regional climate modeling system version 2.0.0*. Retrieved from www.metoffice.gov.uk/precis

Xu, C. H., & Xu, Y. (2012). The projection of temperature and precipitation over China under RCP scenarios using a CMIP5 multi-model ensemble. *Atmospheric Oceanic Science Letter*, *5*, 527–533.

Xu, Y., Gao, X., Shen, Y., Xu, C., Shi, Y., & Giorgi, F. (2009). A daily temperature dataset over China and its application in validating a RCM simulation. *Advances in Atmospheric Sciences*, *26*(4), 763–772. https://doi.org/10.1007/s00376-009-9029-z

Xue, Y., Janjic, Z., Dudhia, J., Vasic, R., & De Sales, F. (2014). A review on regional dynamical downscaling in intraseasonal to seasonal simulation/prediction and major factors that affect downscaling ability. *Atmospheric Research*, *147–148*, 68–85. https://doi.org/10.1016/j.atmosres.2014.05.001

Yu, S., Xia, J., Yan, Z., Zhang, A., Xia, Y., Guan, D., et al. (2019). Loss of work productivity in a warming world: Differences between developed and developing countries. *Journal of Cleaner Production*, *208*, 1219–1225. https://doi.org/10.1016/j.jclepro.2018.10.067

Zander, K. K., Surjan, A., & Garnett, S. T. (2016). Exploring the effect of heat on stated intentions to move. *Climatic Change*, *138*(1), 297–308. https://doi.org/10.1007/s10584-016-1727-9

Zhang, B., Wang, S., & Wang, Y. (2021). Probabilistic projections of multidimensional flood risks at a convection-permitting scale. *Water Resources Research*, *57*(1), e2020WR028582. https://doi.org/10.1029/2020wr028582

Zhao, Y., Sultan, B., Vautard, R., Braconnot, P., Wang, H. J., & Ducharne, A. (2016). Potential escalation of heat-related working costs with climate and socioeconomic changes in China. *Proceedings of the National Academy of Sciences of the United States of America*, *113*(17), 4640–4645. https://doi.org/10.1073/pnas.1521828113

Zhu, J., Huang, G., Wang, X., & Cheng, G. (2017). Investigation of changes in extreme temperature and humidity over China through a dynamical downscaling approach. *Earth's Future*, *5*(11), 1136–1155. https://doi.org/10.1002/2017ef000678

Zhu, J., Wang, S., & Huang, G. (2019). Assessing climate change impacts on human-perceived temperature extremes andunderlying uncertainties. *Journal of Geophysical Research - D: Atmospheres*, *124*(7), 3800–3821. https://doi.org/10.1029/2018jd029444

Zhu, J. X., Huang, G., Wang, X. Q., Cheng, G. H., & Wu, Y. H. (2018). High-resolution projections of mean and extreme precipitations over China through PRECIS under RCPs. *Climate Dynamics*, *50*(11–12), 4037–4060. https://doi.org/10.1007/s00382-017-3860-1